ADVANCED OPTICAL MATERIALS
www.advopticalmat.de



# Improvements of Organic Light-Emitting Diodes Using Graphene as an Emerging and Efficient Transparent Conducting Electrode Material

*Adeniji E. Adetayo, Tanjina N. Ahmed, Alex Zakhidov,* and Gary W. Beall**

Dedicated to Professor Karl Leo on the occasion of his 60th birthday

**Organic light emitting diodes (OLEDs) have received wide attention and progress in impacting the electronics market. The progress of OLEDs in the market over their inorganic counterpart is principally due to their cost savings, flexibility, and excellent performance. As a result of the rising demands for next-generation electronic devices with increased efficiency, high flexibility, reduced cost, and stretchability, there is a need for improvements of OLEDs. In order to fulfill these requirements, it is necessity to replace the transparent conductive electrode (TCE) with a better alternative. The conventionally used TCE, indium tin oxide (ITO), suffers from the scarcity of indium, increased cost, instability, and brittleness. Graphene is recognized as a suitable alternative to ITO because of its excellent properties including high optical transmittance, outstanding electrical conductivity, stability, and great mechanical flexibility. However, the performance of graphene as the TCE material in OLEDs is limited. Several efforts have been made to improve graphene's performance through electrode modifications. This review covers a summary of fabrication techniques for graphene-based TCEs and their improvements. Finally, the application and performance of graphene-based TCEs in OLED devices and the performance of such OLEDs are discussed.**

## 1. Introduction

Organic light emitting diodes (OLEDs) belong to a class of electroluminescent devices fabricated from organic materials (carbon-based), primarily small molecules and polymers. OLED devices are fabricated through the deposition of organic thin film layers by a dry process involving vacuum evaporation of organic materials or a wet process involving a solution coating technique, and they have found extensive utilization in lighting, display, and signage applications (**Figure 1**). The first practical OLED fabricated in 1987 by Tang and VanSlyke[1] from Kodak demonstrated the use of organic materials as a viable alternative to inorganic materials for electroluminescent diodes, which resulted in attractive diode characteristics including ease of fabrication, low production cost, light weight, high-resolution imaging, color tuning ability, wide viewing angle, low operating direct current (DC) voltage, flexibility, thinness, low power consumption, high brightness, fast response, and high electroluminescent efficiency. Since then, increased interest in OLEDs from both academia and industry has emerged due to the rapid development of OLEDs as a major leading technology and owing to their promise for next-generation flat panel displays and solid-state lighting.

The fundamental OLED structure consists of 100–150 nm sized structured layers (conductive and emissive layers) of organic materials sandwiched between a transparent conducting electrode (TCE)—the anode (usually indium tin oxide, ITO) and a cathode (usually Al, Ca, or Ba) all on a transparent substrate (usually plastic or glass). Conventionally, an OLED-stacked structure is composed of a multilayer film stack of a substrate/anode/hole transport layer (HTL)/emissive layer (EML)/electron transport layer (ETL)/cathode. However, device performance in OLEDs has been known to improve through inclusion of other organic layers such as the hole injection layer (HIL), hole blocking layer (HBL), electron injection layer (EIL), and electron blocking layer (EBL) as shown in **Figure 2**a, which is aimed at enabling efficient transportation of charge carriers (holes and electrons) and mitigation of charge trapping for exciton formation. Upon application of an electric potential difference between the two electrodes (anode and cathode) of an OLED device with the transparent conducting anode at a higher positive voltage, positively charged holes from the anode and negatively charged electrons from the cathode are injected and

A. E. Adetayo, T. N. Ahmed, Dr. A. Zakhidov, Dr. G. W. Beall
Materials Science, Engineering, and Commercialization Program
Texas State University
San Marcos, TX 78666, USA
E-mail: alex.zakhidov@txstate.edu; gb11@txstate.edu
A. E. Adetayo, Dr. G. W. Beall
Department of Chemistry and Biochemistry
Texas State University
San Marcos, TX 78666, USA
T. N. Ahmed, Dr. A. Zakhidov
Department of Physics
Texas State University
San Marcos, TX 78666, USA
The ORCID identification number(s) for the author(s) of this article can be found under https://doi.org/10.1002/adom.202002102.

**DOI: 10.1002/adom.202002102**

 

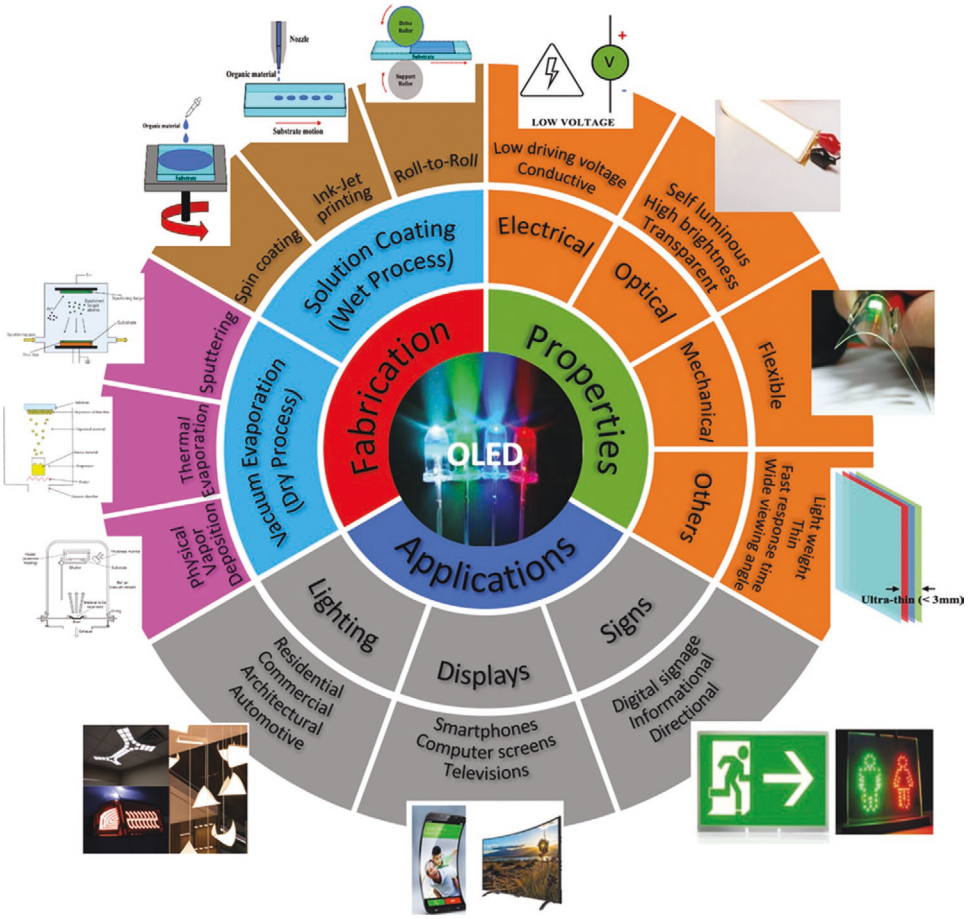


**Figure 1.** Schematic illustration of organic light emitting diode (OLED) from three aspects: fabrication, properties, and applications.

transported through the organic layers comprising the HTL and ETL, respectively, into the EML. Due to the opposing charges of the injected holes and electrons, they get attracted (coulombic attraction) and recombine to form electron–hole pairs in the emissive layer, and the excitons formed relaxes through a photoemissive mechanism to release energy as light (electroluminescence) through the transparent conducting anode (Figure 2b).

TCEs, which are crucial components in OLEDs and other optoelectronic devices, are materials with highly conductive and highly transparent properties. However, with the recent development and need for devices that are foldable and flexible, there has been a need for conducting electrodes that not only meet the requirements for transparency but are also bendable, foldable, and stretchable. Traditionally, conductive metal oxides including ITO and fluorine tin oxide (FTO) are utilized as transparent electrodes in OLEDs. Owing to its excellent optoelectronic properties of high electrical conductivity ($\approx 10^{-4}\ \Omega^{-1}\ cm^{-1}$), low sheet resistance ($R_s$) between 10 and 25 Ω sq.$^{-1}$, and high

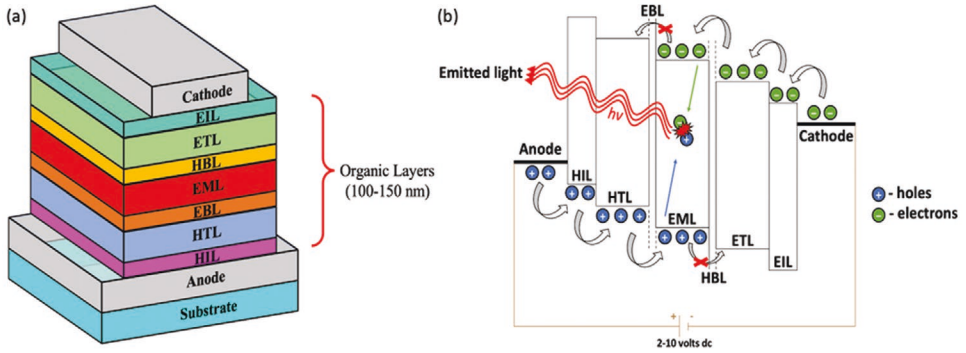


**Figure 2.** a) Multilayered OLED device structure. b) OLED electroluminescence mechanism.

optical transmittance ($T$) over 90% in the visible range, ITO has been the commonly used standard material for TCEs.[2,3] Nevertheless, even with the outstanding properties of ITO, it suffers from some significant setbacks, including the following: i) increased cost of raw material resulting from the global shortage of indium, ii) failures when used in flexible devices owing to its brittle nature, iii) unpleasant high temperature processing during deposition of ITO, iv) instability in acidic and basic environments, and v) poor electrical contact with organic materials. Furthermore, ITO has a considerably high refractive index (≈2.0), which results in undesirable total internal reflection at the ITO/substrate interface when applied on substrates with lower refractive index such as the conventional glass substrate (refractive index ≈1.55) or organic materials (refractive index ≈1.7).[4] Likewise, FTO, which has comparable performance to ITO, is challenged with a reduction in performance (current leakage) at high temperatures caused by high sheet resistance and presence of defects. These shortcomings make the use of conductive metal oxides difficult to meet the growing demand for optoelectronics, specifically OLEDs. To address this demand, many researchers have explored various kinds of materials that meet the major requirements of high optical transmittance, high electrical conductivity, and low sheet resistance as alternatives to ITO for use as TCEs.[5] Other factors of interest include low cost of raw materials, high flexibility for application in flexible devices, and low or room temperature processing for lower costs during fabrication. Many potential materials for ITO replacement have been considered including conducting polymers,[6] metal nanowires (NWs),[7–9] carbon nanotubes (CNTs),[10] and graphene.[11–26] **Table 1** shows the properties and performance of various TCE materials used as anodes in fabrication of OLEDs.

Conducting polymers (CP) such as poly(3,4-ethylenedio xythiophene):poly(styrene sulfonate) (PEDOT:PSS) possess high conductivity and optical transmittance for use as TCEs. Flexibility of these materials makes them suitable for use in applications requiring flexibility. In addition, the ease of fabricating them gives them advantage in fabrication costs. However, since they are made of polymers, they become unstable in unfavorable environmental conditions such as high relative humidity, corrosive environment, and extreme temperatures. This has led to the treatment of PEDOT:PSS with solvents and thermal annealing to enhance their properties and reduce device degradation.[27–29]

Metal nanostructures (NWs, nanofibers, nanogrids, etc.), due to their high conductivity, excellent mechanical flexibility, and high transparency, are excellent materials for TCEs.[7,8,25,30,31] The best performance of TCEs developed from metal nanostructures requires longer and thinner nanomaterials with a high aspect ratio, which is determined by the percolation network.[19] However, silver nanowires (AgNWs) exhibit poor adhesion to substrates, require improvement by strong acid treatment due to poor stability, and require a protection layer to prevent damage from moisture.[7,32,33]

CNTs are a 1D allotropic form of carbon materials formed by rolling individual graphene sheets into a cylindrical structure. They possess high conductivity and are highly transparent in visible wavelengths, making them applicable for use as TCEs. They can also be fabricated easily at a low cost and have outstanding durability in flexible devices.[13,21] However, the use of CNTs is limited by its large sheet resistance resulting from high tube-to-tube contact resistance and the inability to form consistent tubes.[35] Also, properties of CNTs vary largely on the tube type (single-walled nanotubes (SWNTs) and multiwalled nanotubes (MWNTs)), length, and diameter of tube.

Graphene has recently been considered to be a material for TCEs due to its excellent conductivity, high optical transmittance in the visible and near infrared wavelength, great chemical stability, and high flexibility.[13,34,37] Moreover, a single graphene layer benefits from low optical absorbance (≈2.3%), which makes it a unique material for application as a transparent electrode. Transparent conductive electrodes based on graphene are fabricated by chemical vapor deposition (CVD) of graphene from carbon-based materials on a metal catalyst substrate followed by transfer of the graphene film to a flexible substrate.[21,38] This process results in drawbacks such as difficulty in achieving low sheet resistance and wrinkle formation during the graphene transfer process. Contrary to this, a solution-based method of graphene production involving suspension of graphene in liquids has the advantage of lower cost, direct compatibility with flexible substrates, and ease of transfer such as spray coating, spin coating, dip coating, and printing.[39,40] However, while there is an improvement in sheet resistance when compared with the CVD technique, some unwanted defects are also introduced. Even though graphene-based TCEs have excellent properties, low production cost, and ease of fabrication, their sheet resistance of ≈35 Ω sq.$^{-1}$ at 90% transmittance is disadvantageous when compared to the conventional metal-based transparent electrode (ITO) at the same optical transmittance level.[21,34] Also, the use of graphene as the TCE (anode) is limited by its relatively low work function (WF) (≈4.4 eV) compared to ITO (≈4.7 eV). This causes an increase in the injection barrier height at the anode–organic interface.[36] To enhance WF and conductivity of graphene, chemical doping with metal oxides

**Table 1.** Comparison of properties of various materials used as TCEs.

| TCE materials | $R_s$ [Ω sq.$^{-1}$][a)] | $T$ at 550 nm [%][b)] | OLED performance | Mechanical flexibility | Reliability | Low cost | Ref. |
|---|---|---|---|---|---|---|---|
| ITO | 10–25 | >90 | >100 lm W$^{-1}$ | Poor | Good | Poor | [2,34] |
| PEDOT:PSS | 65–176 | 80–88 | 12% EQE | Flexible | Medium | Excellent | [27–29] |
| Silver NWs | 100 | 92 | 54 lm W$^{-1}$ | Flexible | Good | Moderate | [7,32] |
| CNT | 500 | 90 | 10 cd A$^{-1}$ at 1000 cd m$^{-2}$ | Flexible | Excellent | Moderate | [35] |
| Graphene | ≈35 | 90 | 80–103 lm W$^{-1}$ | Most flexible | Excellent | Good | [21,36] |

a) $R_s$, sheet resistance; b) T, transmittance.

($MoO_3$, $WO_3$, and $V_2O_3$) or nitride acids ($HNO_3$) has been carried out.[41–43] Also, multilayered graphene growth shows improvements in the conductivity and WF of graphene.[44,45]

Since TCEs must meet the standard requirement of low sheet resistance and high transmittance for use in devices such as OLEDs, graphene has been comprehensively investigated within the last two decades as an ideal replacement to ITO due to its outstanding properties and excellence performance. Despite the advantages of graphene, its shortcomings restrict its broad adoption for use in organic electronics such as OLEDs. Therefore, to close the gap between theory and practice, many efforts have been made to improve the quality and performance of TCEs. This has involved complementing the limitations of individual material by creating a hybrid material system of different materials available as TCEs in order to combine their properties into a single effective electrode. However, in a pursuit to find a suitable replacement for ITO, most materials have involved improvements of TCEs in OLEDs by improving graphene quality through chemical doping to minimize the high sheet resistance and hybridizing ITO alternatives, including conducting polymers such as PEDOT:PSS, metal NWs, and CNTs with graphene, graphene oxide (GO), or reduced graphene oxide (rGO).[46–48] OLED devices fabricated using graphene-based TCE material show huge potential for replacement of rigid devices with next-generation lighting and display devices that are flexible, foldable, and even stretchable with increased functionality and performance. Thus, this review covers the characteristic properties of transparent conductive electrodes including low sheet resistance and high transparency, with the measure for comparison of these properties being the figure of merit (FOM) to establish material performance and efficiencies in OLEDs. We will also describe the structure and properties of graphene and its derivatives that make it a unique material. In addition, we provide a summary of the synthesis methods for graphene and its derivatives (GO and rGO) that have previously been investigated for use as TCEs, as well as the improvements in the performance of graphene-based TCEs by chemical doping or combination with other materials to form a hybrid structure for application in OLED optoelectronic devices with optimum performance. We hope that the information on the advancement of graphene and its derivative as a suitable TCE material for the improvement of OLED devices summarized in this review will enhance the development and commercialization of next-generation highly efficient and flexible OLED devices for successful transition from rigid to flexible electronic devices.

## 2. Property Requirements for TCE and Performance Evaluation

### 2.1. Conductivity and Optical Transmittance

The major properties for consideration in TCE selection are conductivity and optical transmittance. For excellent performance of TCEs, high conductivity and high transparency are critical requirements. However, it is difficult to achieve high optical transmittance and high conductivity simultaneously; therefore, there is always a trade-off.

Conductivity, $\sigma$ (S $cm^{-1}$ or $\Omega^{-1}$ $cm^{-1}$), is the ability of a material to allow the flow of electricity while resistivity ($\rho = 1/\sigma$) is the ability of a material to oppose such flow. Thus, for a material to have high conductivity, the resistivity must be minimized. A material with a high conductivity must have high charge carrier density, i.e., concentration of charge carriers and/or high carrier mobility, $\mu$. Equation (1) gives the expression for conductivity

$$\sigma = en\mu_e + ep\mu_h \tag{1}$$

where $e$ is the electron charge ($1.6 \times 10^{-19}$ C), $n$ and $p$ are the density of charge carriers ($n$ for electrons and $p$ for holes) in $m^{-3}$, $\mu_e$ and $\mu_h$ are electron mobility and hole mobility, respectively, in $m^2$ $V^{-1}$ $s^{-1}$, and $\sigma$ is the DC conductivity.

Due to the negligible size of electrons, they move faster than holes, and as such, good conductors have electrons as their charge carriers. Resistivity, $\rho$, of thin film is measured in terms of its sheet resistance, $R_s$, as given by

$$R_s = \frac{\rho}{t} = \frac{1}{\sigma t} \tag{2}$$

where $t$ is the thickness of the film in nanometers (nm). Increase in film thickness results in an increase in conductivity and a decrease in resistivity. However, with a thicker film, there is an increase in optical absorption that affects the optical transmittance, $T$

$$T = e^{-\alpha t} \tag{3}$$

where $\alpha$ is the optical absorption coefficient. As the thickness of a film increases, the optical transmittance decreases, resulting from the film losing transparency (**Figure 3**a).[21] In the case of graphene, the optical transmittance is reduced by ≈3%, as shown in Figure 3a.

For a bulk film, the sheet resistance is given by

$$R_s = \frac{1}{\sigma_{DC,B} t} \tag{4}$$

where $\sigma_{DC,B}$ represents the bulk DC conductivity. Combining Equations (3) and (4) to eliminate $t$, the relationship between $T$ and $R_s$ is given by

$$T = e^{-\frac{\alpha}{\sigma_{DC,B}} R_s} \tag{5}$$

This shows that for bulk films, the value of sheet resistance, $R_s$, for a given transmittance, $T$, is controlled by the ratio of the bulk DC conductivity to the absorption coefficient, $\sigma_{DC,B}/\alpha$. Equation (5) is only applicable for freestanding films.[49] In the case of nanostructure materials (nanotubes, NWs, graphene, etc.), percolation in these films is accounted for by the introduction of a percolation exponent. For this case, sheet resistance as defined by De et al. [50] is given by

$$R_s = \frac{1}{\sigma_{DC,B}\left(\frac{t}{t_{min}}\right)^n t} = \frac{1}{\sigma_{DC,B}\left(\frac{t^{n+1}}{t_{min}}\right)} = \frac{t_{min}^{n+1}}{t_{min}\sigma_{DC,B}t^{n+1}} \tag{6}$$

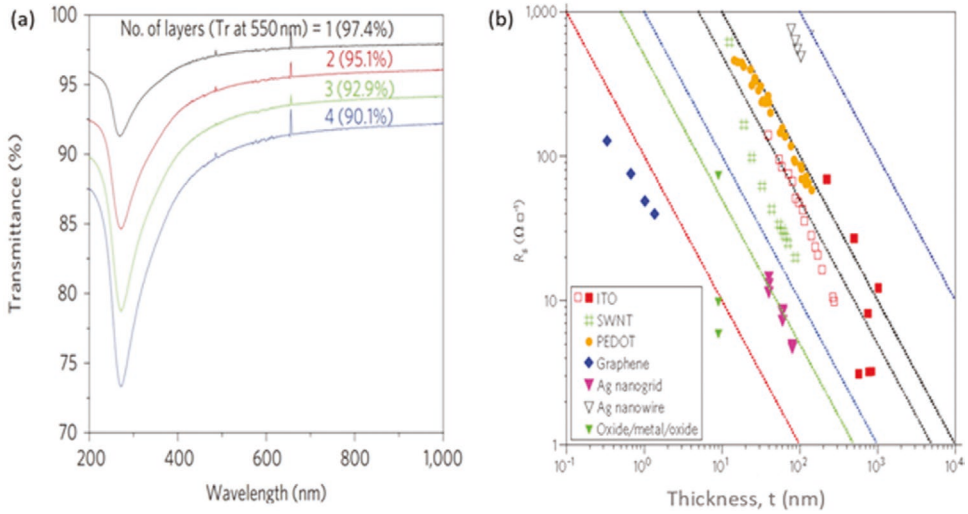


**Figure 3.** a) Spectral transmittance for graphene films at varied number of layers (one to four). Reproduced with permission.[21] Copyright 2010, Springer Nature. b) Sheet resistance $R_s$ as a function of film thickness t for different films: Ag, Al, and Cu metal grids; PEDOT:PSS; ITO films; SWNTs; Ag nanogrids; oxide/Ag/oxide films; and graphene. The dotted lines correspond to constant resistivities, $\rho$ of $1 \times 10^{-5}$, $5 \times 10^{-5}$, $1 \times 10^{-4}$, $5 \times 10^{-4}$, $1 \times 10^{-3}$, and $1 \times 10^{-2}$ Ω cm (from left to right). Reproduced with permission.[22] Copyright 2012, Springer Nature.

where $n$ is the percolation exponent and $t_{min}$ is the critical thickness ($t_{min} > 20$ nm) below which nanostructure materials no longer behave like bulk and the DC conductivity decreases with decreasing thickness.[51]

Figure 3b shows the relationship between sheet resistivity, $R_s$, and film thickness, $t$, for different TCEs. As expected from Equation (1), the data agree with $R_s$ varying inversely with $t$. Constant resistivity lines ranging from $10^{-5}$ to $10^{-2}$ Ω cm were also plotted. Graphene films displayed the lowest resistivities (≈$5 \times 10^{-6}$ Ω cm), closely followed by oxide/Ag/oxide films (≈$7 \times 10^{-6}$ Ω cm), Ag nanogrids (≈$5 \times 10^{-5}$ Ω cm), and SWNTs (≈$3 \times 10^{-4}$ Ω cm). The obtained ITO data (red filled boxes) for thickness, $t > 100$ nm, are a little higher in resistivity (≈(2–5) $\times 10^{-4}$ Ω cm), than the best ITO films today (red open boxes) with the same thickness and resistivity ≈$10^{-4}$ Ω cm. PEDOT:PSS films and AgNWs displayed the highest resistivity values.

### 2.2. Figure of Merit

TCEs require materials with high conductivity, high optical transmittance, and low sheet resistance. However, in most materials such as graphene, there is always a trade-off as the best performance for a TCE is often obtained with a combination of high conductivity, low sheet resistivity, and lower optical transparency. Thus, a criterion that could compare the properties of TCEs and determine their performance is essential. FOM has been developed to serve this purpose. With several approaches to determine the FOM for TCEs reported, different equations have been set up by many researchers.[49,50,52–58] However, none of the equations is the established method to determine the FOM. Presented in this paper are the commonly used FOM equations applied in most studies to evaluate the performance of TCEs.

Haacke[53] provided an expression for FOM ($\Phi_{TC}$) by combining the electrical and optical properties (sheet resistance, $R_s$, and optical transmission, $T$) of materials given by

$$\Phi_{TC} = \frac{T^x}{R_s} = T^x \sigma t \tag{7}$$

where $x$ is an exponent selected based on required transmittance. To maximize $\Phi_{TC}$, film thickness, $t$, must be maximized, i.e., $t_{max} = (x\alpha)^{-1}$, where $\alpha$ is the optical absorption coefficient. An $x$ value of 10 is usually a sufficient choice since most transparent conductor applications typically require no more than 90% (0.9) optical transmittance. At 90% transmittance, the FOM is expressed as

$$\Phi_{TC} = \frac{T^{10}}{R_s} = T^{10} \sigma t \tag{8}$$

The film thickness dependent FOM developed by Haacke is often used to predict transparent electrode properties of materials, as it simplifies numerical calculations of practical FOM.

Another approach to compare TCE materials involves the use of transmittance in the visible wavelength regime to evaluate their performance. This FOM is given by dividing the material's DC conductivity, $\sigma_{DC,B}$, by the optical conductivity, $\sigma_{OP}$[59]

$$\frac{\sigma_{DC}}{\sigma_{OP}} = \frac{Z_0}{2} \frac{\sqrt{T}}{R_s\left(1-\sqrt{T}\right)} = \frac{188.5\sqrt{T}}{R_s\left(1-\sqrt{T}\right)} = \frac{188.5}{R_s\left(T^{-1/2}-1\right)} \tag{9}$$

where $Z_0$ is the impedance of free space (377 Ω), $\sigma_{OP}$ is the conductivity due to motion of electrons in optical fields, and $\sigma_{DC,B}$ is the conductivity by charge transport as a result of constant applied fields. In most studies, transmittance, $T$, has been taken in the visible range of 550 nm as this corresponds

to the maximum human visual sensitivity. The FOM can be maximized for high transmittance at a specific sheet resistance. Unlike Equation (8), this FOM is thickness independent and applicable to a wider range of films. However, it is not suitable for nanostructure films as a result of percolation, which needs to be accounted for as stated earlier, and as such, it is only appropriate for freestanding films.[49]

Generally, the higher the FOM, the better the performance of the TCE irrespective of the FOM equation used. For industrial purposes, TCEs require a sheet resistance, $R_s \approx 100\ \Omega$ sq.$^{-1}$, at transmittance greater than 90%. For device fabrication, specifically OLEDs, ITO serves as the basis for comparison with $R_s = 10\ \Omega$ sq.$^{-1}$ at transmittance $T > 90\%$. Thus, using this as a benchmark to determine performance of TCEs, the benchmark FOMs from Equations (8) and (9) are $\approx 3.49 \times 10^{-2}\ \Omega^{-1}$ and ≈350, respectively.

### 2.3. Device Quality of OLEDs

Transparent conductive electrodes are used in fabrication of several organic electronic devices including OLEDs and organic photovoltaics (OPV). Particularly, in the case of OLED devices, a voltage bias is applied to generate the emission of light as opposed to OPV devices where light is inputted to generate a voltage. Thus, to obtain best performance of OLEDs, the TCEs utilized in the device have to be optimized. Several approaches to determine the performance of OLED devices exist in the form of efficiencies. The efficiency of an OLED is characterized by its quantum efficiency in percentage (%), the current efficiency ($\eta_L$) in cd A$^{-1}$, or the luminous efficiency ($\eta_P$) in lm W$^{-1}$.

#### 2.3.1. Quantum Efficiencies in OLEDs

The quantum efficiency of a device includes the internal quantum efficiency, IQE ($\eta_{int}$), and the external quantum efficiency, EQE ($\eta_{ext}$). The EQE is the number of emitted photons per number of injected charges and is given by

$$\eta_{ext} = \eta_r \phi_f \chi \eta_{out} = \eta_{int} \eta_{out} \tag{10}$$

where $\eta_r$ is the probability of holes ($p$) and electrons ($n$) recombining to form excitons. This can approach the value of unity in organic materials as there is a low mobility of charge carriers causing less probability for formation of excitons. However, OLED efficiency is based on the efficiency of the injection of holes and electrons into the organic layers. Consequently, $\eta_r$ needs to be maximized by having a good balance of holes and electrons. $\phi_f$ is the fluorescent quantum efficiency, i.e., the fraction of excitons that radioactively decay. For organic materials, this can approach 100%. $\chi$ is the probability for radioactive decay to occur. Only singlet excitons exist for light emission. In conventional fluorescent devices, $\chi$ is generally confined to 25%, implying only 25% of excitons can produce light.[60] However, in polymer materials, this can be of higher values. $\eta_{out}$ is the fraction of photons that escape the device as determined by waveguiding in the device layers and substrate. In planar structures such as OLEDs, $\eta_{out} \approx 1/(2n^2)$, where $n$ is the refractive index (≈1.7 for organics). $\eta_{out}$ is usually ≈20%. In classical OLED systems (fluorescent OLEDs), the EQE is ≈4–5%.[60]

#### 2.3.2. Macroscopic Efficiencies in OLEDs

The luminance ($L$) in cd m$^{-2}$ is the amount of light emitted from a given device area. Macroscopic efficiencies of OLEDs include current efficiency ($\eta_L$) and luminous efficiency ($\eta_P$).

The current efficiency ($\eta_L$) in cd A$^{-1}$ is the luminance ($L$) in cd m$^{-2}$ per current density ($J$) in A m$^{-2}$ flowing into the diode and is given by

$$\eta_L = \frac{L}{J} \tag{11}$$

The luminous efficiency ($\eta_P$) in lm W$^{-1}$ is the optical flux per electrical input and is given by

$$\eta_P = \frac{L\pi}{JV} = \eta_L \frac{\pi}{V} \tag{12}$$

where $V$ is the working voltage.

OLED devices require high luminance and high luminous efficiency, which involves a combination of high current efficiency and low voltage. In the design of OLEDs, it is important to consider human response as the human eye is more sensitive to some colors than others. $\eta_L$ and $\eta_P$ are maximum in the green range, and therefore the human eye responds much better to green light than to blue and red light, which have lower $\eta_L$ and $\eta_P$. Therefore, current and luminous efficiencies must be tuned to specific wavelengths of light in order to adjust for how the human eye perceives the emitted color.

## 3. Structure of Graphene, Graphene Oxide, and Reduced Graphene Oxide

Graphene, a 2D single layer structure of carbon atoms arranged in a honeycomb lattice structure, has received tremendous scientific interest following the first successful isolation of a single layer of graphite (i.e., graphene) on a substrate by peeling highly ordered pyrolytic graphite on a sticky tape by Geim and Novoselov.[61] It is an allotropic form of carbon that may be constructed to form other carbon allotropic forms such as 0D fullerene formed by wrapping graphene to form a sphere (buckyball), 1D CNT formed by rolling graphene to form a cylinder, and 3D graphite formed by stacking graphene as illustrated in **Figure 4**. These various forms of carbon exhibit various properties due to their various atomic orientations.

Graphene exhibits attractive anisotropic properties including high intrinsic carrier mobility (≈200 000 cm$^2$ V$^{-1}$ s$^{-1}$), theoretically large surface area (2630 m$^2$ g$^{-1}$), excellent optical transmittance (≈97.7%), high thermal conductivity (≈5000 W m$^{-1}$ K$^{-1}$), high Young's modulus (≈1.0 TPa), very high electrical conductivity, and ability to withstand high current density.[62–64] These exciting properties of graphene and its derivatives (GO and rGO) have led to its use in various applications including OLEDs.

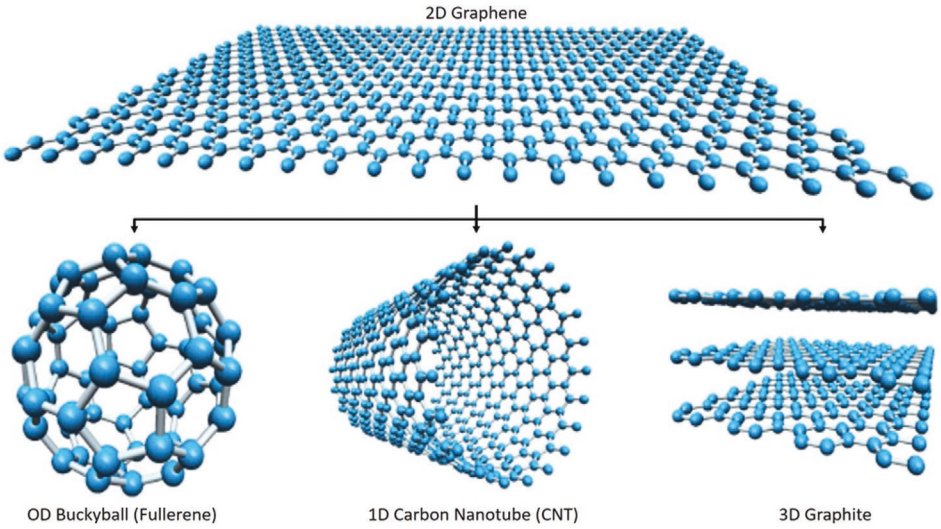


**Figure 4.** Illustration of 2D graphene as a building block for other carbon allotropic dimensions.

GO results from the chemical oxidation of graphite followed by exfoliation. This results in GO with many oxygen functional groups attached to carbon. With chemical reduction of GO, most of the functional groups are removed as a result of alterations in chemical structure leading to the formation of rGO similar in structure to pristine (defect-free) graphene (**Figure 5**a). The process for reduction of GO is illustrated in Figure 5b. Although the electronic properties of rGO are greatly affected by the presence of residual oxygen functional groups resulting in structural defects, it still finds various applications due to its low cost of production and ease of transfer onto substrates.

## 4. Fabrication of Graphene-Based Transparent Conducting Film

Several synthesis methods to obtain graphene have been employed for use in various applications. Fabrication techniques such as mechanical exfoliation of graphite (scotch tape method), liquid-phase exfoliation, chemical reduction of GO,[65–68] CVD by hydrocarbon,[69–71] epitaxial growth on electrically insulating surfaces such as SiC, and total organic synthesis have been extensively studied and detailed in several review articles.[72–74] The classification of each method is summarized in **Figure 6**.

Although graphene produced through mechanical exfoliation produces the highest quality graphene in a simple way, it is challenged with extremely low yield, limited reproducibility, and inadequate scalability. Toxicity and structural damage of graphene film are the major concerns for the liquid-phase exfoliation technique. Furthermore, the impossibility of transfer of graphene grown on the SiC surface and the rigorous method used in total organic synthesis make the production of graphene films for use as transparent electrodes very challenging. Currently, the most commonly used methods to fabricate transparent conductive graphene films are CVD and chemical reduction of GO.

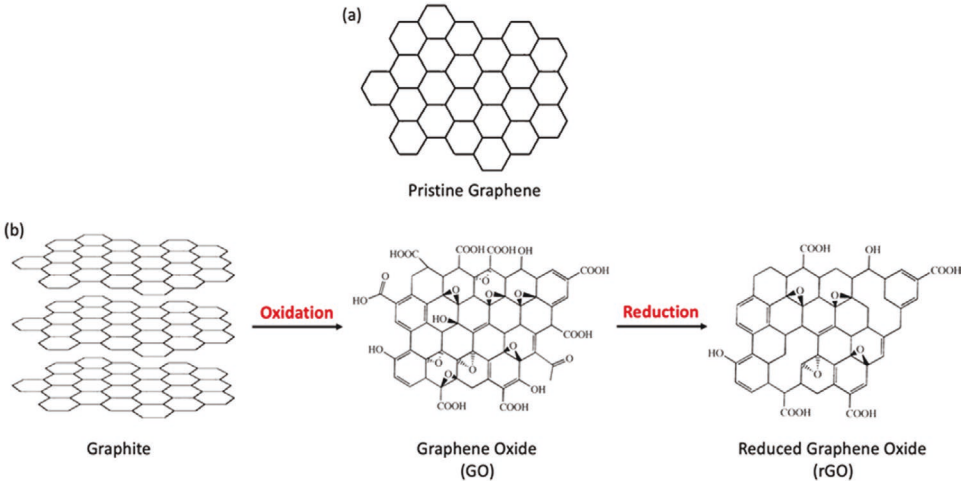


**Figure 5.** a) Structure of defect-free (pristine) graphene. b) Synthesis of reduced graphene oxide (rGO) from intermediate graphene oxide (GO).

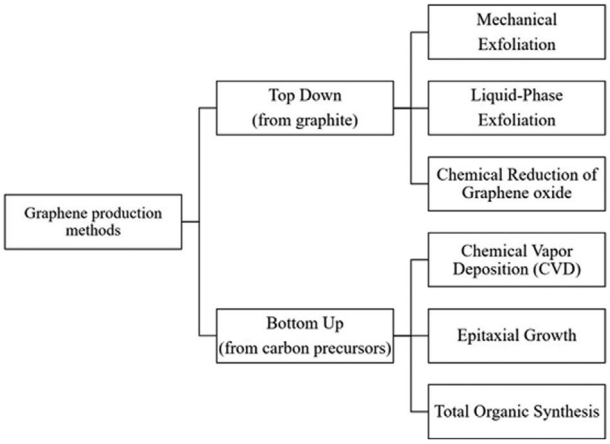


**Figure 6.** Graphene synthesis methods.

### 4.1. Chemical Vapor Deposition

CVD is the most-used technique to produce high-quality graphene in large area. This synthesis method involves flowing buffer gases and hydrocarbon precursor gas for decomposition of carbon onto a transition metal catalyst substrate in a furnace at high temperature (≈500–1000 °C). A schematic representation of this technique is shown in **Figure 7**.

With this technique, graphene is usually grown on transition metal substrates such as Cu, Ni, Pt, Ru, and Ir using carbon precursors including methane, acetylene, and benzene.[75–78] This is followed by graphene transfer from the underlying metal layer onto arbitrary substrates like glass for use as TCEs.[79] Generally, the growth mechanism and number of graphene layers (monolayer, bilayer, or multilayer) are dependent on the type of metal substrate, the type and flow rate of gases, reaction time, pressure, and temperature.

Kim et al. demonstrated the CVD growth of graphene on Ni metal catalyst at 1000 °C using methane, hydrogen, and argon gas.[69] Rather than formation of graphene films, thick graphite (multiple graphene layers) was formed due to the absorption of a large amount of carbon as shown in **Figure 8**a. However, high carbon solubility of Ni resulted in the formation of multilayer graphene. Wrinkles and rough surface morphology were observed because of the thermal expansion coefficient difference between graphene and Ni catalyst (Figure 8a, inset). To suppress the formation of multiple layers, thin layers of nickel and rapid cooling were applied, resulting in the separation of

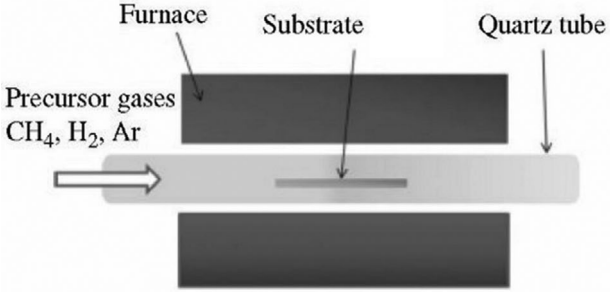


**Figure 7.** Schematic representation of CVD technique.

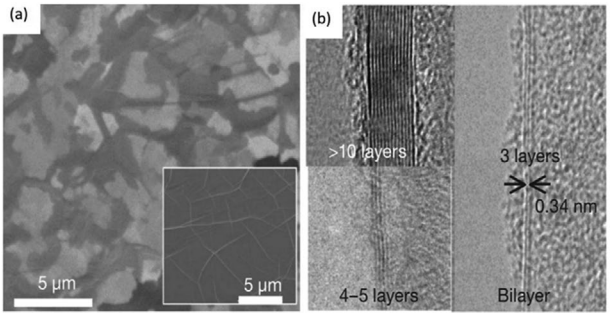


**Figure 8.** CVD growth of graphene on Ni metal catalyst. a) Scanning electron microscopy (SEM) image; b) transmission electron microscopy (TEM) image. Reproduced with permission.[69] Copyright 2009, Springer Nature.

graphene layers from the nickel substrate. Transmission electron microscopic images (Figure 8b) confirmed the formation of a mixture of monolayer, bilayer, and multilayer graphene.

Unlike nickel, CVD growth of graphene on copper substrate demonstrated by Li et al. showed increased monolayer coverage over 90% for large-scale synthesis using methane at 1000 °C.[71] This process results from the decomposition and adsorption of carbon atoms on the surface of Cu, which forms nucleation sites for other carbon atoms leading to the growth of graphene film as described in **Figure 9**. The rapid cooling process enhances the formation of monolayer graphene across the Cu substrate.[71]

The growth mechanism of CVD graphene on Ni occurs via carbon dissolution and segregation, whereas graphene growth on copper is by surface adsorption owing to its low carbon solubility making it possible to grow monolayer graphene.[80,81] Similarly, due to the thermal expansion differences, graphene growth on Cu substrates results in wrinkles and rough morphology.[78] Also, Chen et al. demonstrated the large-scale CVD synthesis of graphene on Cu–Ni alloy.[82] By varying the atomic fraction of Ni in Cu, the carbon solubility was controlled to produce monolayer and multilayer graphene.[82–85]

Graphene films grown on catalytic metal substrates to be used as TCEs require a critical step involving the transfer of graphene films from metal substrate onto a transparent substrate such as glass or polyethylene terephthalate (PET).[13,79,86–92] Conventionally, a wet transfer process involving polymers such as polydimethylsiloxane (PDMS)[69,93] or poly(methyl methacrylate) (PMMA)[94,95] is commonly used to transfer graphene. These polymers act as support and strength for graphene to protect it from damage during the transfer process. This transfer process involves coating the surface of the metal catalyst substrate (Cu or Ni) with the polymer (PDMS or PMMA) followed by etching of the metal substrate with an appropriate chemical etchant ($FeCl_3$, $Fe(NO_3)_3$, HCl, $HNO_3$, etc.). Residual etchant is removed from the polymer/graphene film using deionized (DI) water, and the clean polymer/graphene film is transferred to the transparent substrate in DI water. The polymer support is then removed by organic solvents (acetone and isopropyl alcohol) with a little residual polymer left on the transparent substrate for use as a transparent electrode.[79,89,96] The conventional PMMA transfer method is shown in **Figure 10**a. This wet transfer process creates some defects and wrinkles

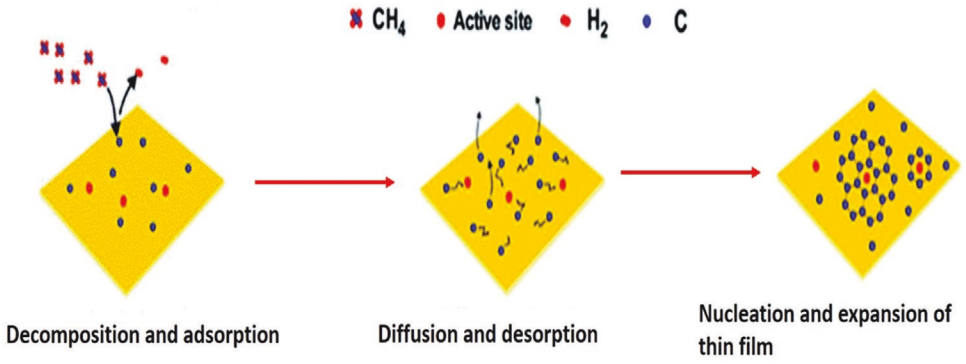


**Figure 9.** Flow chart of the CVD growth mechanism of graphene on Cu substrate.

in the transferred graphene, which results in the yield being affected.[97] To circumvent this, several techniques have been investigated to effectively transfer graphene onto arbitrary substrates. Bae et al. developed a technique for graphene transfer by using a thermal release tape (TRT).[21] This was demonstrated by using a roll-to-roll-based transfer process assisted by TRT. The graphene/Cu film is first attached to the TRT in the first lamination process followed by etching of Cu foil in the second roll process, and then the TRT/graphene transfer of CVD graphene onto target substrate by heating to remove TRT in the third lamination process as shown in Figure 10b. Repeated treatment using this technique produces thicker graphene films with thickness being proportional to the number of cycles.

To date, copper is the most utilized substrate for CVD growth of monolayer graphene. Sheet resistance ($R_s$) depends on the graphene transfer process as shown in **Figure 11** and doping, which is discussed in section 5.1 of this paper. $R_s$ for the roll-to-roll transferred monolayer graphene with TRT support is about two times larger than the conventional PMMA assisted transferred monolayer graphene (125 Ω sq.$^{-1}$ at 97.4% optical transmittance). With an increase in cycle of the roll-to-roll technique to form thicker graphene, the resistance rapidly drops from ≈275 Ω sq.$^{-1}$ until it reaches a resistance value of ≈40 Ω sq.$^{-1}$ for four-layer graphene film, which is similar to the four-layer graphene wet transferred with PMMA.[21] Furthermore, there is an effective improvement in the conductivity of monolayer graphene compared to the thick graphene film through $HNO_3$ doping. For monolayer graphene, conductivity is improved by ≈50% as the layer increases to two while the four-layer graphene shows an improvement of ≈25% as shown in Figure 11a. Interestingly, with $HNO_3$ doping, the sheet resistance of the four-layer graphene film was reduced from ≈40 to ≈30 Ω sq.$^{-1}$ at an optical transmittance of 90%. This makes CVD graphene superior to conventional ITO used as a transparent electrode as shown in Figure 11b. Also, graphene has high flexibility unlike ITO, which produces microcracks when a strain is applied.[21]

Raman spectra of CVD graphene transferred using the wet process is shown in Figure 11c. This displays characteristic monolayer graphene peaks at ≈1350, ≈1580, and ≈2680 cm$^{-1}$ corresponding to the D-band, G-band, and 2D-band, respectively.[21] These Raman signatures are representative of phonon scattering and provide important information which dictates graphene's film quality, presence of structural defects, number of graphene layers, thickness, and domain size. The D-band is an in-plane vibrational mode originating from intervalley phonon scattering due to the presence of defects (i.e., disorder-induced peak). The G-band is a different in-plane vibrational mode and the single first-order peak in graphene while the 2D-band is the second-order double resonance of the D-band

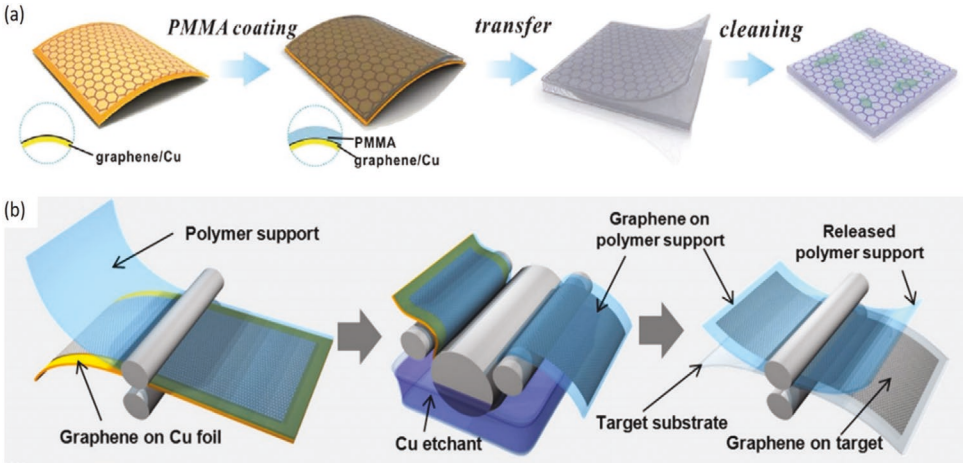


**Figure 10.** Transfer process of CVD graphene. a) Conventional PMMA assisted transfer. Reproduced with permission.[161] Copyright 2014, Royal Society of Chemistry. b) Roll-to-roll transfer with TRT support. Reproduced with permission.[21] Copyright 2010, Springer Nature.

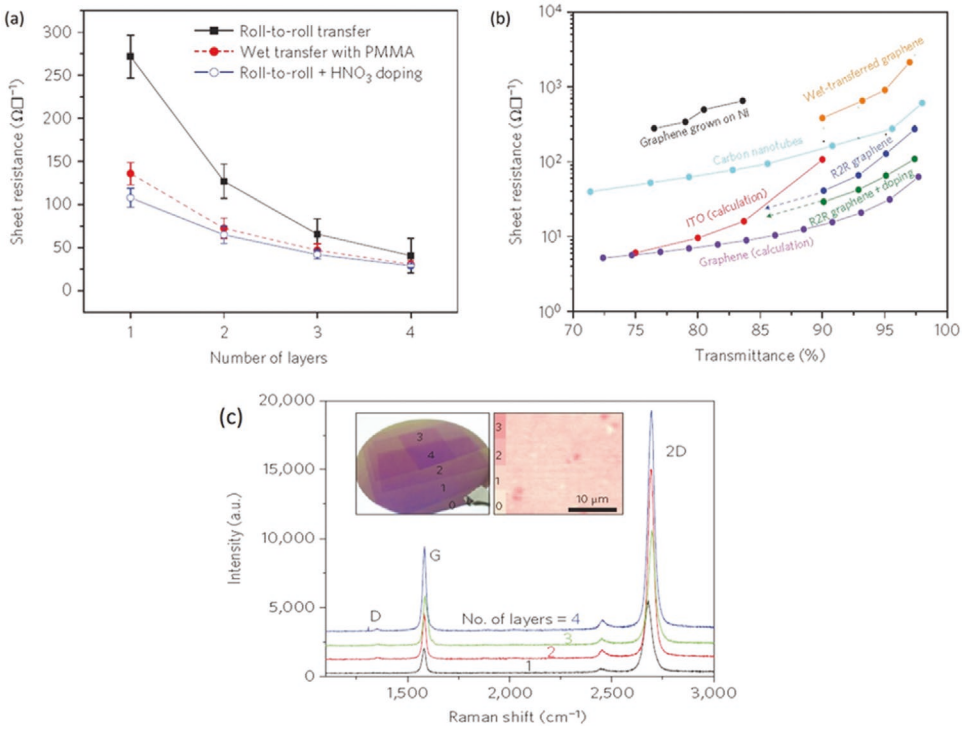


**Figure 11.** a) Sheet resistances of different graphene transferred films by different transfer methods (roll-to-roll transfer assisted with TRT, PMMA assisted wet transfer, and roll-to-roll with $HNO_3$ doping); b) comparison of sheet resistances of different TCEs; c) Raman spectra of CVD graphene films at varied number of layers (one to four). Left inset shows a picture of PMMA transferred graphene layers on $SiO_2$/Si wafer. Right inset shows optical micrograph of graphene with 95% monolayer coverage. Reproduced with permission.[21] Copyright 2010, Springer Nature.

(i.e., D-band overtone) which is present but independent of the presence of defects. The level of disorder in graphene and graphene quality can be estimated using the $I_D/I_G$ intensity ratio while the $I_{2D}/I_G$ intensity ratio reflects the number of graphene layers.

As result of low intensity of the D peak in Figure 11c, there is low lattice disorder resulting in low defects of graphene. However, as the number of layers increases, the intensity of the G and 2D peaks increase with their ratios not having a significant change due to random stacking of each layer. Also, there is a slight shift in the position of G and 2D peaks while the peak shape is preserved.[21]

Several other techniques of CVD graphene transfer have been investigated. Cai et al. examined the growth of graphene on a transparent polymer substrate using a low-pressure CVD technique.[98] With the nonremoval of polymer substrate, a successful crackless transfer of graphene film with $R_s$ of 219 Ω sq.$^{-1}$ at optical transmittance of 96.5% was achieved. This produced graphene film of about five times higher than the conductivity of undoped graphene film transferred with polymer removal.[98] Using the dealuminated process, Chandrashekar et al. transferred graphene films prepared by the CVD technique on Cu foil onto polymeric substrate.[99] The etch-free transfer using roll-to-roll green technique resulted in sheet resistance of 5.2 kΩ sq.$^{-1}$ at optical transmittance of 97.5% for undoped graphene with a reduction in damage. Efforts have also been made on the direct growth of graphene on glass substrates.[96,99–101] As demonstrated by Sun et al., catalyst-free atmospheric CVD (APCVD) growth of uniform graphene film with large area was directly grown on glass substrate.[100] This resulted in graphene with sheet resistance of ≈370–510 Ω sq.$^{-1}$ at an optical transmittance of 82%. Using various dielectric substrates coated with nickel-carbon thin film, monolayer graphene was grown using rapid thermal process by Xiong et al., resulting in a sheet resistance of 50 Ω sq.$^{-1}$ at transmittance of 96%.[102] Though this process resulted in low resistance at high transmittance, it was not applicable to plastic and glass substrates due to high processing temperature up to 1100 °C.

Graphene production via the CVD technique, although, is challenged with limitation on the choice of substrate, critical transfer process, high sheet resistance, and difficulty in thickness regulation, it is still the best graphene film production method used for TCE as it is easily compatible with industry since it is widely used, and the sheet resistance, which is of critical importance, is by far better than the ones reported by other graphene synthesis methods.

### 4.2. Reduction of Graphene Oxide

Aside from the CVD technique, another technique for graphene production for TCEs is the reduction of GO. This technique offers large-scale production and a low-cost method of graphene film production involving oxidation of graphite with strong acids followed by exfoliation in water to yield GO. GO is then deposited onto a desired substrate and reduced through thermal or chemical means.[103–105]

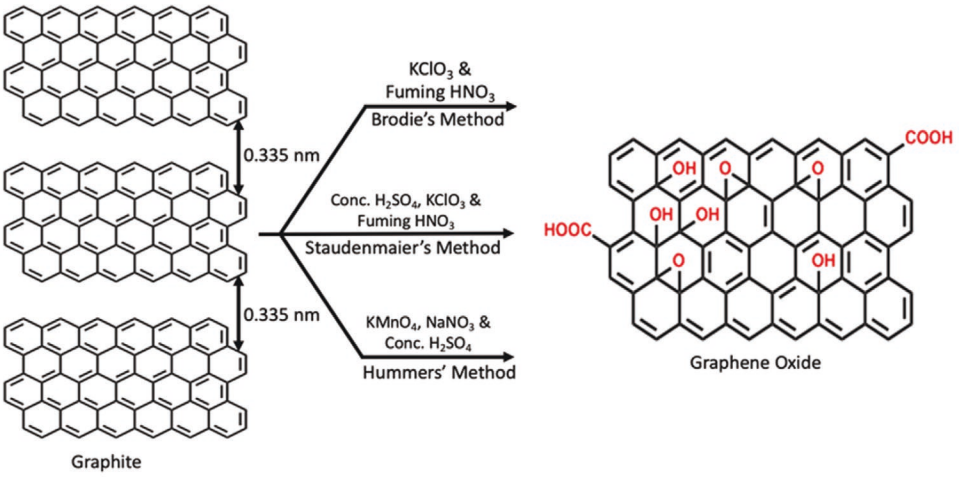


**Figure 12.** Synthesis routes of graphene oxide from graphite. Reproduced with permission.[74] Copyright 2019, Scientific Research Publishing.

Due to the presence of oxygen groups, GO is hydrophilic, resulting in suspension and easy dispersion in water and various organic polar solvents. This makes it easy to produce large-area film at a low cost.

Generally, oxidation of graphite to synthesize GO can occur by Brodie's method,[106] Staudenmaier's method,[107] or Hummers'[68] method as shown in **Figure 12**.

Hummers' method has been the most commonly used method for oxidation of graphite. Graphite oxide produced through this method exhibits increased interlayer spacing, and upon ultrasonication, the interlayer spacing is further increased resulting in GO with individual layer suspensions. Through the oxidation process, epoxy and hydroxyl groups are formed in the base plane and carboxyl groups at the edges (Figure 12). The presence of these functional groups results in some disorder in the electronic structure and reduced electrical conductivity compared to pristine graphene (defect-free).

Following the oxidation process, GO suspension is transferred onto the preferred substrate to fabricate the GO films. This can be achieved through dip coating,[103] spray coating,[108] spin coating,[109] vacuum filtering,[65,66] or the Langmuir-Blodgett (L–B) technique.[110]

Spray coating and dip coating are the easiest ways to deposit the GO suspension on the arbitrary substrate. Gilje et al. utilized the spray coating technique to transfer GO onto preheated substrate.[108] This resulted in immediate deposition of GO platelets on the substrate following the evaporation of the solvent to prevent clustering of GO platelets and ensure uniformity of film.[108] Due to the easy, quick, high yield, and scalability of spray coating, it is the most suitable method for large-scale production processes.[111,112]

Dip coating involves the immersion of a substrate in a GO suspension followed by draining of suspension and drying of substrate.[103]

The spin coating technique provides uniform and continuous GO films but requires high concentrations (0.5–3 mm $mL^{-1}$). However, it is more convenient as the thickness of GO films can be easily determined by the concentration of GO dispersion and the spin coating speed/cycle.

However, due to high flexibility of GO sheets, spray, dip, and spin coating techniques produced sheets with wrinkles, and aggregation of GO platelets was difficult to avoid.

Vacuum filtration involves the deposition of GO suspension onto a cellulose ester membrane followed by transfer of GO film to an arbitrary substrate and etching of ester membrane with acetone solvent. Eda et al. utilized the vacuum filtration technique to deposit GO film on a glass substrate using an ester membrane.[65,66] By controlling the filtration volume, the thickness and sheet resistance varied. The sheet resistance decreases dramatically with an increase in filtration volume after annealing but saturates at a critical volume due to the reduction being effective for only the top few layers as seen in **Figure 13**a.[66] rGO obtained using hydrazine vapor and low temperature annealing (200 °C) had a sheet resistance of 70 kΩ $sq.^{-1}$ at low transmittance of 65% (Figure 13b).[65]

The L–B method is a sophisticated technique in which GO sheets are floated on the water/air interface and isopropanol or methanol is added to the solution slowly.[110] This is then compressed by L–B trough, leading to a gradual increase in surface pressure. Continuous and uniform film is obtained on reaching the desired pressure, resulting from the electro-repulsive force between carboxyl functional groups at the edges exceeding the electro-attractive force in the base plane (epoxy and hydroxy).[110] The GO film is then deposited on the desired substrate by lifting it from the solution.

After successful deposition of GO films on the desired substrate, it is necessary to reduce the insulating GO film in order to restore its destroyed $sp^2$ carbon network and conductivity. In general, reduction of GO films is achieved through chemical reduction and thermal reduction at high temperature. Chemical reduction of GO is achieved using various reducing agents such as hydrazine, hydrazine vapor, sodium borohydride, hydroxylamine, amino acid, ascorbic acid, and urea.[109,113,114] However, the chemical reduction process is not a complete restoration technique as there is a residual of functional groups resulting from the irreversibly destroyed $sp^3$ carbon and vacancies acting as electron traps.[115] Consequently, thermal reduction at high temperature has been considered to be a more efficient way for reduction of GO.[116] Unfortunately, due to the high temperature

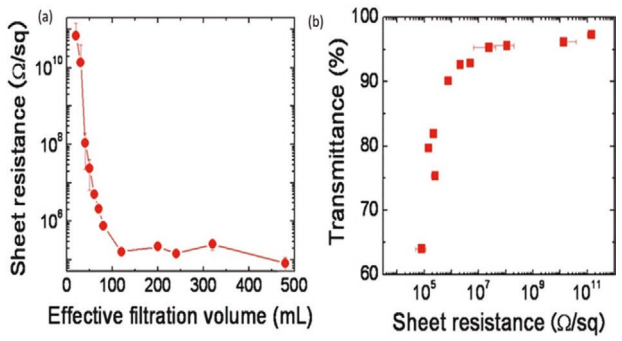


**Figure 13.** a) Sheet resistance of rGO films as a function of filtration volume. Reproduced with permission.[66] Copyright 2008, Springer Nature. b) Transmittance as a function sheet resistance for rGO films. Reproduced with permission.[65] Copyright 2008, AIP Publishing.

requirement (above 1000 °C) for a long period of time, it is not applicable to substrates that cannot withstand high temperature such as plastic substrates used in flexible TCEs. Various methods have been reported to reduce GO including electrochemical reduction,[117] hydrothermal reduction,[118] microwave assisted reduction,[119] and photochemical reduction.[120]

## 5. Improvements of Graphene-Based Transparent Conductive Film

Graphene has been shown to have excellent properties for use as a transparent conductive electrode to replace conventional ITO; however, several factors determine its properties and performance as a TCE such as the fabrication technique and transfer method. Various methods produce graphene electrodes with differences in electrical conductivity, sheet resistance, WF, and transmittance. To improve the properties of graphene as a TCE, several approaches have been made including doping of graphene and hybridizing graphene with other materials.

### 5.1. Doping

Prepared graphene films have been shown to exhibit good electrical conductivity and high optical transmittance; however, their sheet resistance still remains high. This affects its use as a TCE material. To solve this, graphene usually undergoes postchemical doping after its transfer to the desired substrate, which changes the type and increases the charge carrier concentration, thus reducing the sheet resistance. Chemical doping involves the substitution of carbon atoms by introduction of impurities to the graphene.[121,122] Graphene can be p-type or n-type doped based on the position of the fermi level of graphene, the highest occupied molecular orbital (HOMO), and the lowest unoccupied molecular orbital (LUMO) of the doping. Decreasing the fermi level of graphene below the HOMO (doping with larger electron negativity materials), a p-type doping occurs as the hole transfer moves from the dopant to the graphene. Increasing the fermi level of graphene above the LUMO (doping with larger electron positivity materials), an n-type doping occurs as the electron transfers from the dopant to the graphene. Doping of graphene has been achieved by using $HNO_3$,[121,123] $Fe(NO_3)_3$,[124] $FeCl_3$,[125] $AuCl_3$,[126–128] $Na^+$,[129] $SOCl_2$,[123,130] 1-pyrenebutanoic acid succinimidyl ester,[131] bromine,[132] urea,[133] etc.

Doping of graphene using acids and salts is an effective route to decreasing sheet resistance of graphene while maintaining its transparency. Using $HNO_3$ or $AuCl_3$ increases WF of graphene while decreasing the sheet resistivity for OLEDs.[36] Using $AuCl_3$ redox dopant, sheet resistance of a four-layer graphene film was decreased to as low as 30 Ω sq.$^{-1}$ and was utilized as anodes for OLEDs with increased luminous efficiency, luminance, and current efficiency. For a trilayer graphene film, sheet resistance of 150 Ω sq.$^{-1}$ was achieved at transmittance >91%.[134] Doping of a few-layer graphene with $FeCl_3$ enhanced conductivity with reduced sheet resistance of 8.8 Ω sq.$^{-1}$ at 84% transmittance.[135]

*P*-doping of graphene has also been achieved using tetracyanoquinodimethane ($C_{12}H_4N_4$) to increase hole carrier concentration and decrease sheet resistance.[136] Also, n-doping of graphene using pentaethylenehexamine ($C_{10}H_{28}N_6$) reduced sheet resistance of graphene by up to ≈400% compared to pristine graphene.[137] Polyvinyl alcohol also achieved n-doping of graphene to reduce sheet resistance from ≈4 to ≈400 Ω sq.$^{-1}$ without affecting its transmittance.[138]

### 5.2. Hybridized Graphene-Based Films

Graphene and other conductive materials can be combined to overcome the challenges faced by the individual material and improve the performance of graphene as TCE. Common materials used in the hybridization of graphene include CNTs, metal nanostructures, and conducting polymers. Combining these materials as a single functional film helps to enhance the electrical conductivity and optical performance of the films for use as TCEs.

#### *5.2.1. Hybridization with CNT*

To overcome the challenges discussed earlier in the use of graphene and CNT as transparent electrodes, a composite material can be formed in which the network of NWs provides an electronic pathway to bridge the percolating bottleneck, such as high resistance grain boundary, leading to reduced resistance at high transparency.[139–141]

Kim et al. developed a graphene hybrid film by CVD growth of graphene on Cu foil coated with SWNTs.[139] This graphene/SWNT hybrid electrode displayed superior properties with sheet resistance of 300 Ω sq.$^{-1}$ at a 96.4% transparency compared to spin coated graphene/SWNT with a resistance of 1100 Ω sq.$^{-1}$ at a 96.2% transmittance.[140] A double layer rGO/MWNT hybrid structure was also demonstrated to exhibit a resistance of 151 kΩ sq.$^{-1}$ at 93% transmittance for a 60 μg mL$^{-1}$ concentration of MWNT dispersion.[142]

#### *5.2.2. Hybridization with Metal Nanostructure*

Due to the inability of metal nanostructures to withstand high temperature and current, they have the limitation of early

failure rates.[143] To avoid this, they can be combined with graphene to form an individual film with graphene ameliorating this drawback. Also, the defects in graphene from grain boundaries leading to its high resistance can be complemented by forming a graphene–metal hybrid structure.[144]

Zhu et al. synthesized a graphene/metal grid hybrid structure placed onto PET film with resistance of ≈20 Ω sq.$^{-1}$ at a transmittance of 90%.[145] CVD graphene with a network of AgNWs has also shown low sheet resistance of 22 Ω sq.$^{-1}$ at an optical transmittance of 88% with outstanding stability.[146] Damage from the atmosphere was enhanced even after four months with a 13 Ω sq.$^{-1}$ sheet resistance. Ahn et al. developed a rGO/AgNW hybrid electrode that can withstand high temperature and long stability with a sheet resistance slightly increasing even at 70 °C and relative humidity of 70% for eight days.[147]

#### *5.2.3. Hybridization with Conducting Polymer*

A graphene/PEDOT:PSS hybrid structure has been fabricated by several researchers due to its extremely high flexibility for use as TCEs.[148–150] Stable suspension of a rGO was produced through chemical reduction of GO in the presence of PEDOT:PSS to form a rGO/PEDOT:PSS hybrid electrode by Jo et al.[148] TCE film exhibited a sheet resistance of 2.3 Ω sq.$^{-1}$ at 80% optical transmittance. Liu et al. developed a graphene/PEDOT:PSS hybrid ink to produce high-quality graphene at a large scale.[150]

In summary, formation of hybrid TCEs with graphene has a significant effect on improving the electronic and optical properties of optoelectronics such as OLEDs when compared to ITO-based TCEs. Additionally, these hybrid films have the advantages of flexibility and stability. Nevertheless, techniques used to fabricate graphene, other materials, and the hybrid film determine the properties of such TCEs. The optoelectronic properties of TCEs developed using graphene are summarized in **Table 2**.

## 6. Application of Graphene-Based TCEs in OLEDs

OLEDs are used today as displays for phones, television screens, watches, and computer display, and in many other applications. The commercial ITO used as the anode suffering from inferior flexibility and instability has prompted a lot of research to find a replacement for ITO in OLEDs. Graphene films due to their high flexibility, electrical conductivity, and transparency have demonstrated their promise as a candidate for replacing ITO. Several reports have demonstrated this promise.[36,40] A conventional OLED structure of anode/PEDOT:PSS/*N*,*N*′-di-1-naphthyl-*N*,*N*′-diphenyl-1,1′-biphenyl-4,4′diamine (NPD)/tris(8-hydroxyquinoline) aluminum ($Alq_3$)/LiF/Al was adopted to investigate the performance when a graphene film was used as the transparent electrode.[40] A sheet resistance of ≈800 Ω sq.$^{-1}$ at a transmittance of 82% was obtained. **Figure 14**a,b shows the device performance. The OLED exhibited a turn-on voltage of 4.5 V compared to ITO with 3.8 V turn-on voltage. It also reached a luminance of 300 cd m$^{-2}$ at 11.7 V.[40] Han et al.[36] also demonstrated the enhancement of OLEDs based on graphene transferred on PET substrate and acid doping as shown in Figure 14c–f. Sheet resistance and WF of undoped graphene varied from 189 to 87 Ω sq.$^{-1}$ and ≈4.3–4.4 eV respectively as a function of the number of layers varying from two to four. The luminance also increased as a function of graphene layers. Four-layered graphene devices with $AuCl_3$ doping displayed higher luminance attributed to higher conductivity

**Table 2.** Properties of transparent conducting electrodes (TCE) based on graphene-based materials.

| Material | Details | Deposition/transfer techniques | $R_s$ [Ω sq.$^{-1}$] | Transmission [%] | Ref. |
|---|---|---|---|---|---|
| CVD graphene | $HNO_3$ doping | Dry transfer/TRT | ≈30 (four layers) | 90 | [21] |
| | Cu catalyst | Roll-to-roll green transfer | 5.2k | 97.5 | [99] |
| | Ni catalyst | Wet transfer | 500 | 75 | [38] |
| | Ni/C on dielectrics | Transfer-free growth | 50 | 96 | [102] |
| | Cu–Ni alloy | Wet transfer | 409 | 96.7 | [82] |
| rGO | Thermal reduction of GO | Spin coating | $10^2$–$10^3$ | 80 | [109] |
| | | Filtration | 43k | 95 | [66] |
| | | Dip coating | ≈1.8k | 70.7 | [103] |
| Graphene/CNT | Graphene on SWNT | Wet transfer | 300 | 96.4 | [139] |
| | CVD | Wet transfer | 600 | 95.8 | [142] |
| | Thermal reduction of rGO on MWNT | Electrostatic adsorption | 151k | 93 | [142] |
| | Chemically converted graphene/SWNT suspension | Spin coating | 636 | 92 | [151] |
| | Ultralarge GO/SWNT | Langmuir–Blodgett | 180–560 | 77–86 | [152] |
| Graphene/NW | CVD graphene on AgNW | – | 22 | 88 | [141] |
| | AgNW on graphene | – | 33 | 94 | [87] |
| | Graphene/CuNW | – | 25 | 82 | [143] |
| Graphene/polymer | Graphene/PEDOT:PSS hybrid ink | Spray coating | 600 | 80 | [150] |
| | rGO/PEDOT:PSS hybrid ink | Filtration | 2.3k | 80 | [148] |
| | PEDOT:PSS support layer on CVD graphene | Wet transfer | 80 ± 4 | 84.6 | [149] |

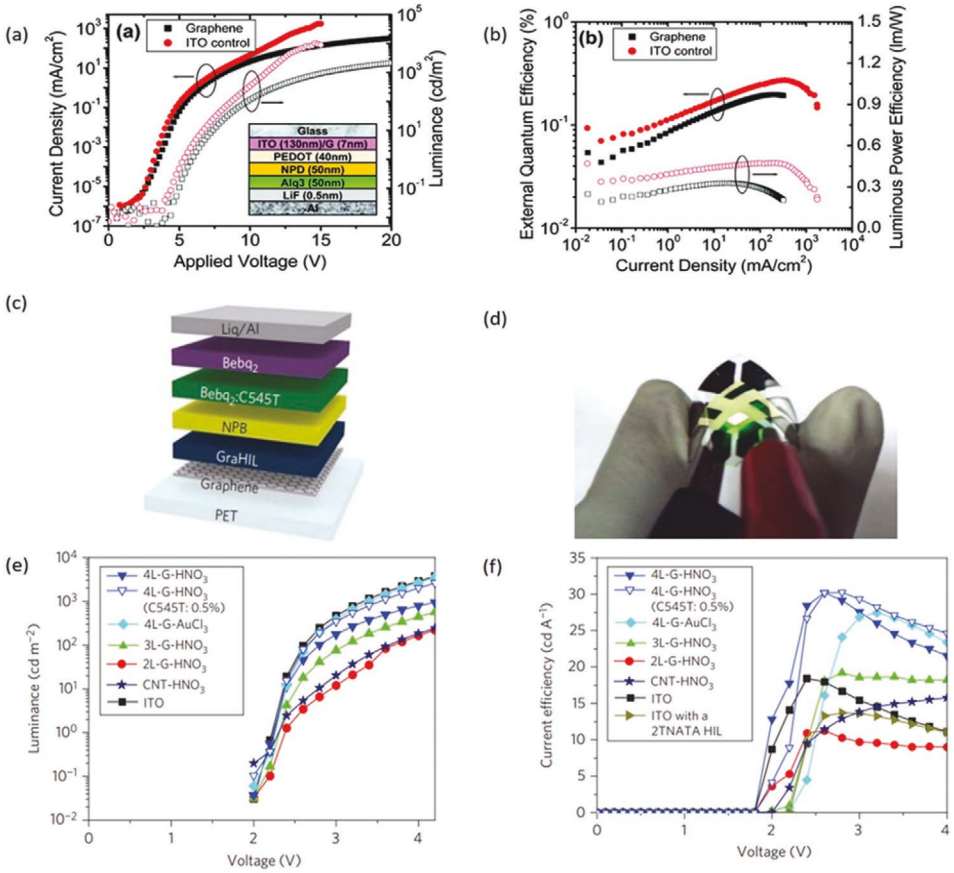


**Figure 14.** a) Current density (solid filled symbols) and luminance (open symbols) versus applied voltage for graphene and ITO-based OLEDs. Inset shows the device structure. Reproduced with permission.[40] Copyright 2010, American Chemical Society. b) External quantum efficiency (EQE) (solid filled symbols) and luminous power efficiency (open symbols) for graphene and ITO-based OLEDs. Reproduced with permission.[40] Copyright 2010, American Chemical Society. c) Device structure of fluorescent OLEDs. Reproduced with permission.[36] Copyright 2012, Springer Nature. d) Optical image of light emission from a flexible fluorescent green OLED with a four-layered graphene anode (4L-G) doped with $HNO_3$ (4L-G-$HNO_3$). Reproduced with permission.[36] Copyright 2012, Springer Nature. e) Luminance versus applied voltage of OLED devices with various doped graphene layers. Reproduced with permission.[36] Copyright 2012, Springer Nature. f) Current efficiency versus applied voltage of OLED devices with various doped graphene layers. Reproduced with permission.[36] Copyright 2012, Springer Nature.

and WF (34 Ω sq.$^{-1}$ and ≈5.1 eV respectively) as compared to $HNO_3$-doped devices (54 Ω sq.$^{-1}$ and ≈4.6 eV respectively).[36] $HNO_3$- and $AuCl_3$-doped devices with four-layered graphene showed significantly higher maximum current efficiencies (30.2 cd A$^{-1}$ with $HNO_3$ doping, 27.4 cd A$^{-1}$ with $AuCl_3$ doping) when compared to ITO-based devices.

Transition metal oxide film of molybdenum trioxide ($MoO_3$) has also been investigated for the p-doping of graphene and compared to the performance of ITO in OLEDs by Meyer et al.[42] In their work, OLEDs with the device structures as shown in **Figure 15**a were fabricated to understand band engineering, interfacial charge transfer effects of $MoO_3$ doping of graphene electrodes, and performance of graphene-based OLEDs. Thermal evaporation of thin layers of $MoO_3$ (<5 nm) in between the electrode/organic interfaces resulted in a large 1.9 eV interface dipole and the down bending of the conduction band of $MoO_3$ closer to the graphene Fermi level, resulting in a close to ideal alignment of the energy levels and a 0.25 eV increase in WF of graphene.[42]

With efficient charge transfer doping of graphene, sheet resistance varied from ≈700 to 30 Ω sq.$^{-1}$ for monolayer to four-layer graphene, and transmittance ranging between 94% and 86% for monolayer and four-layer graphene respectively.[42] Figure 15b,c shows the device characteristics of OLED fabricated using monolayer graphene compared to ITO and Figure 15d,e represents devices fabricated with three-layer graphene electrode. The devices displayed a similar turn-on voltage of 2.5 V for both graphene-based and ITO-based OLEDs. Graphene-based OLEDs indicated higher current efficiencies of 55 and 67 cd A$^{-1}$ for monolayer and three-layer graphene-based devices respectively at luminance of 1000 cd m$^{-2}$.[42] The graphene-based OLED working device is shown in Figure 15f. Tungsten trioxide ($WO_3$) which has better stability to air exposure than $MoO_3$ was similarly utilized for doping monolayer graphene in the graphene-based OLED stack comprising anode/$WO_3$/$WO_3$ doped 4,4′-Bis(N-carbazolyl)–1,1′-biphenyl (CBP)/CBP/CBP doped bis(2-phenylpyridine)(acetylacetonate)iridium(III) [Ir(ppy)$_2$(acac)]/1,3,5-tris-phenyl-2-benzimidazolyl-benzene (TPBi)/8-hydroxy-quinolinato lithium (Liq)/Al.[43] As $WO_3$ layer thickness increased, sheet resistance decreased to around < 300 Ω sq.$^{-1}$ and a 0.2 eV downshift in

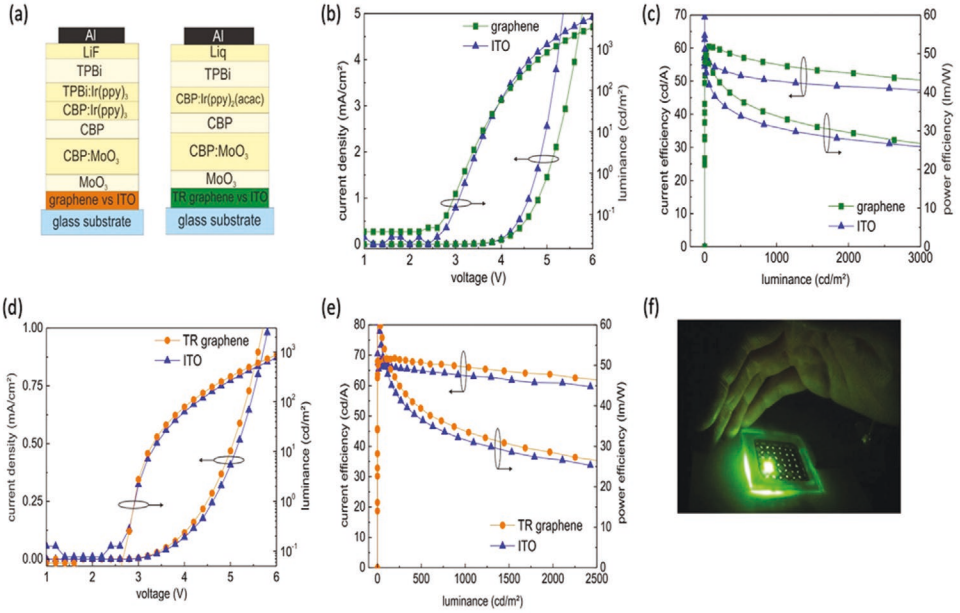


**Figure 15.** a) OLED device structure stacks. b) Current density and luminance versus applied voltage for monolayer graphene and ITO-based OLEDs doped with $MoO_3$. c) Current efficiency and power efficiency versus luminance for monolayer graphene and ITO-based OLEDs doped with $MoO_3$. d) Current density and luminance versus applied voltage for three-layer graphene and ITO-based OLEDs doped with $MoO_3$. e) Current efficiency and power efficiency versus luminance for three-layer graphene and ITO-based OLEDs doped with $MoO_3$. f) Graphene-based OLED with high brightness. Reproduced with permission.[42] Copyright 2014, Springer Nature.

the Fermi level, similar to $MoO_3$ doped graphene by Meyer et al. [42,43] The OLED characteristic as shown in **Figure 16**a,b shows a higher operating voltage for the graphene-based device with 5 nm thick layer of $WO_3$ when compared to ITO (2.7 V), and reduced power efficiency of 50 lm $W^{-1}$ at luminance of 1000 cd $m^{-2}$ resulting from an increased sheet resistance of graphene during oxygen plasma treatment. Increasing $WO_3$ thickness to 15 nm improved the device performance of graphene-based OLED with a slightly higher power efficiency (≈62 lm $W^{-1}$) when compared to ITO (60 lm $W^{-1}$) at luminance of 1000 cd $m^{-2}$.[43] Wu et al. [41] studied the use of substitutionally boron-doped monolayer graphene as a suitable anode for OLED devices using the device architecture as shown in Figure 16c. Sheet resistance (240 Ω $sq.^{-1}$), optical transmittance on glass (97.5% at 550 nm), and WF (5.0 eV) of boron-doped graphene was superior to pristine graphene (350 Ω $sq.^{-1}$, 97.7%, and 4.7 eV respectively) and ITO anodes.[41] To demonstrate the use of boron-doped graphene for flexible OLED devices, boron-doped graphene on PET substrate was subjected to bending radius of 0.75 mm for 3000 bend cycles. Negligible change in sheet resistance ratio as shown in Figure 16d suggests high stability of boron-doped graphene and suitability for flexible OLEDs. Fabricated boron-doped graphene OLEDs exhibited excellent performance as shown in Figure 16e,f with maximum EQE of 24.6%, maximum current efficiency of 95.4 cd $A^{-1}$, and maximum power efficiency of 99.7 lm $W^{-1}$.[41]

Using PEDOT:PSS conducting polymer, the low work function and high sheet resistance of graphene can be improved to enhance their performance in OLEDs. Shin et al. fabricated OLEDs on glass substrate using a hybrid anode composed of monolayer graphene/PEDOT:PSS and compared their performance to graphene anode OLED.[46] Graphene/PEDOT:PSS film yielded a sheet resistance of 90 Ω $sq.^{-1}$ with an optical transmittance of 92.8%, comparable to the sheet resistance of 1500 Ω $sq.^{-1}$ and transmittance of 96.4% obtained with graphene film. It is believed that the introduction of PEDOT:PSS helps to form a continuous conductive path in graphene and provides mechanical protection that minimizes the negative effect of defects and wrinkles during the graphene transfer process. With the addition of spin coated PEDOT:PSS onto graphene, a WF gradient from the graphene to the hole injection layer was created to enhance hole injection and reduce the hole injection barrier at the anode/hole injection layer interface of the graphene/PEDOT:PSS-based OLED. The hybrid anode OLED was reported to display enhanced performance with a maximum current efficiency of 0.89 cd $A^{-1}$ and maximum luminance of 735.4 cd $m^{-2}$ at 15.0 V as shown in **Figure 17**a,b.[46] Similarly, electrodes with double-layered graphene/PEDOT:PSS conductive film was used by Wu et al. to fabricate flexible OLEDs.[153] The hybrid electrode on a PET substrate showed highly conductive with light-emitting stability upon bending due to the presence of graphene and a negligible change in sheet resistance (≈300 Ω $sq.^{-1}$) during the bending test at 10 mm radius (Figure 17c). Smoothening of the rough surface morphology of pure graphene film was achieved by spray coating PEDOT:PSS, which reduced sheet resistance by ≈390 Ω $sq.^{-1}$ and prevents rapid device degradation of OLEDs.[153] Figure 17d,e,f shows the performance of graphene/PEDOT:PSS-based flexible OLEDs with a turn-on voltage of 5 V, maximum current efficiency of 0.91 cd $A^{-1}$, and negligible degradation in current efficiency upon severe bending.

The presence of grain boundaries in CVD graphene films limits its conductivity and charge carrier concentration, these unwanted grain boundaries result in poor performance in

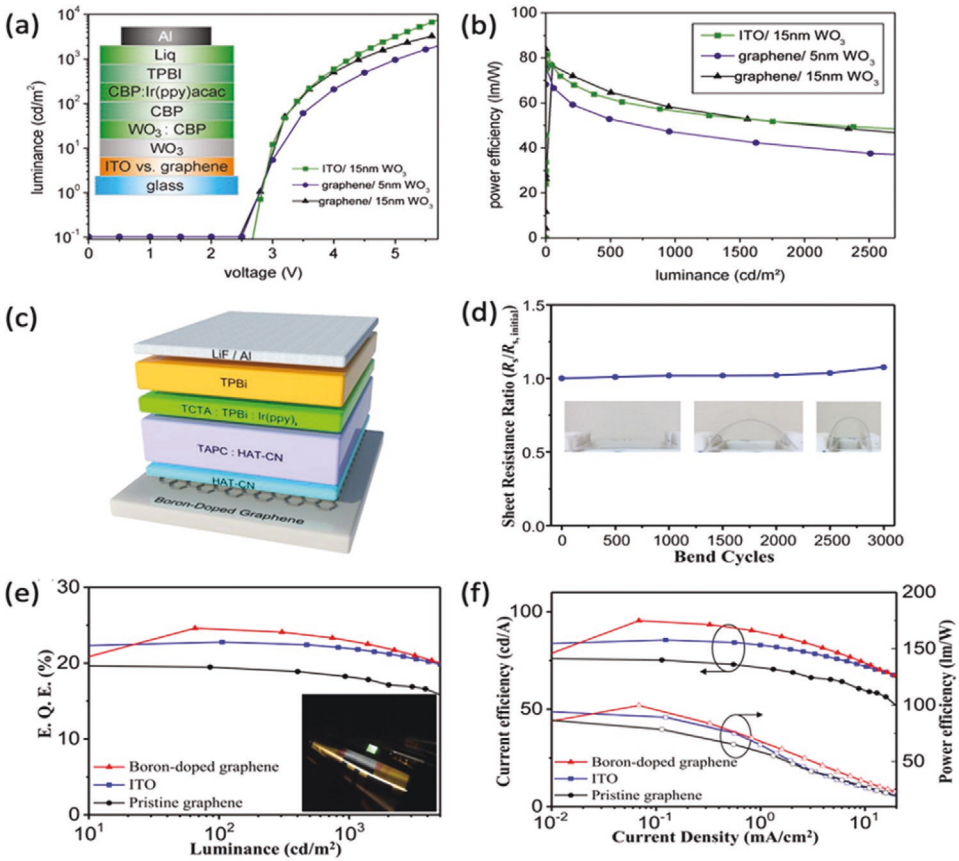


**Figure 16.** a) Luminance versus applied voltage. Inset shows the OLED device structure stack. Reproduced with permission.[43] Copyright 2015, AIP Publishing. b) Power efficiency versus luminance for monolayer graphene and ITO-based OLEDs doped with $WO_3$. Reproduced with permission.[43] Copyright 2015, AIP Publishing. c) Device structure of OLED fabricated with boron-doped graphene. Reproduced with permission.[41] Copyright 2017, American Chemical Society. d) Sheet resistance ratio versus bend cycles for boron-doped graphene on PET substrate. Inset shows the optical picture of bent samples. Reproduced with permission.[41] Copyright 2017, American Chemical Society. e) EQE versus luminance for boron-doped graphene, ITO, and pristine graphene OLEDs. Inset shows illuminated flexible boron-doped OLED device. Reproduced with permission.[41] Copyright 2017, American Chemical Society. f) Current efficiency and power efficiency versus current density for boron-doped graphene, ITO, and pristine graphene OLEDs. Reproduced with permission.[41] Copyright 2017, American Chemical Society.

optoelectronic devices. Reduction of the effect of grain boundaries of graphene can be minimized by creating a conductive pathway using AgNWs to connect the graphene nanosheets and provide a positive "bridge effect" for electron transport as demonstrated by Li et al. in **Figure 18**a.[144] In their work, flexible OLEDs were fabricated using single layer graphene (SLG)/AgNWs hybrid electrode as shown in Figure 18b. The hybrid SLG/AgNWs film resulted in the reduction of sheet resistance of graphene from 650 to 27 Ω sq.$^{-1}$ at an optical transmittance of 86.7% and WF of 5.1 eV, surpassing conventional ITO electrodes. Fabricated OLEDs with SLG/AgNWs electrode also displayed a turn-on voltage of 2.5 V, maximum luminance of 15 000 cd m$^{-2}$ at 9 V, and an increase in current density from 55 to 107 mA cm$^{-2}$ at 9.5 V when compared to SLG (Figure 18c).

A flexible hybrid electrode composed of monolayer graphene/silver nanowires/polymer matrix (MG–A–P) was also developed to overcome the weakness and challenges of bare electrodes.[47] With increasing AgNWs concentrations, the optical transmittance of MG–A–P film was slightly lower than the A–P film due to the addition of the monolayer graphene. However, based on performance as TCEs, the FOM obtained using Equation (8) for MG–A–P film exhibited superior optoelectronic properties with largest FOM value of $35.7 \times 10^{-3}$ Ω$^{-1}$ at a sheet resistance value of 8.06 Ω sq.$^{-1}$ and transmittance of 88.3% as shown in **Figure 19**a.[47] Completely encapsulating AgNWs between graphene and mixed polymer matrix prevented corrosion and oxidation of AgNWs, thereby improving the stability of the hybrid electrode. Figure 19b shows the bending test of different electrodes subjected to 2.0 mm radius of curvature. MG–A–P film displayed minimum change in sheet resistance with no cracking after 300 bending cycles, indicative of its suitability for flexible optoelectronic devices. The brittle nature of ITO results in a drastic increase in the relative resistance change upon bending due to microcracks being formed, thereby limiting the performance of ITO-based OLEDs. In particular, this is the biggest obstacle in the use of ITO for the development of flexible OLEDs. Flexible OLEDs fabricated using GN–A–P hybrid electrode as shown in Figure 19c device structure outperformed ITO-based devices with turn-on voltage of 3.38 V, maximum brightness of 4297 cd m$^{-2}$, and maximum current efficiency of 2.11 cd A$^{-1}$ (Figure 19d–f).[47]

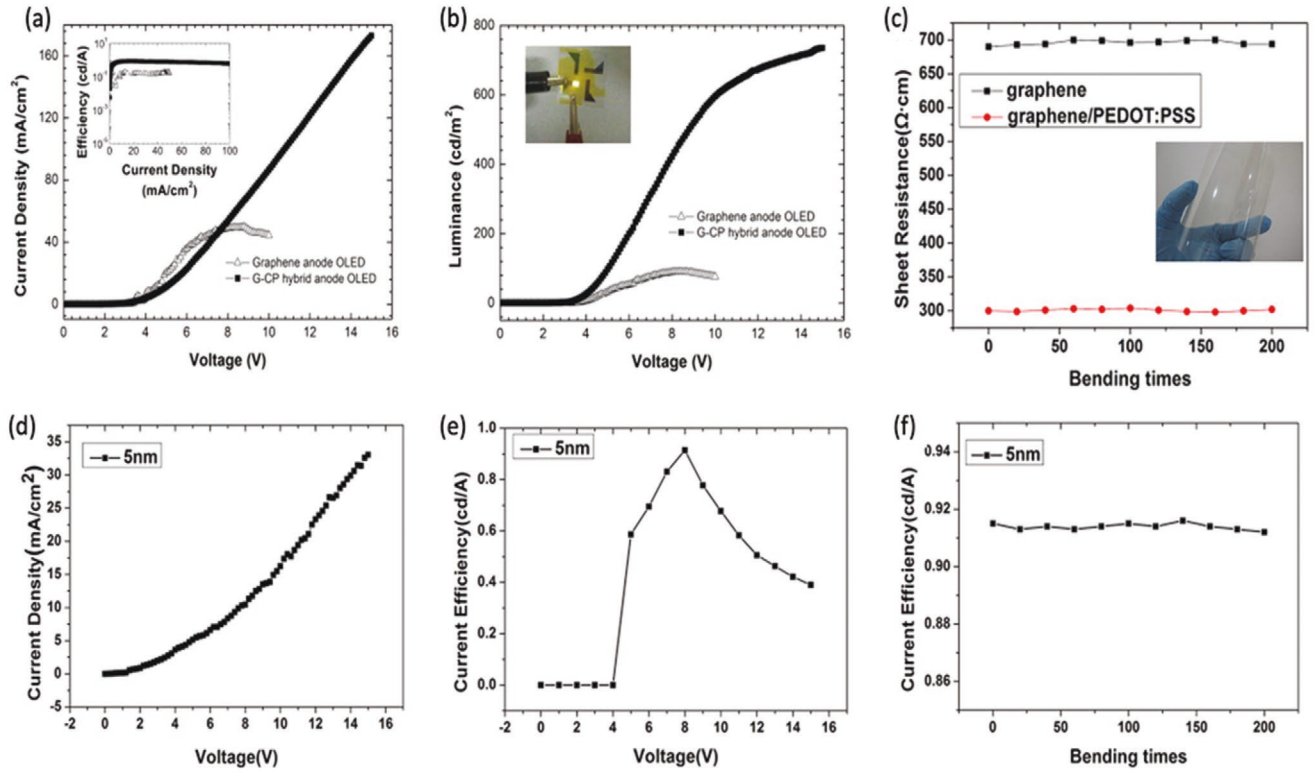


**Figure 17.** a) Current density versus applied for monolayer graphene and monolayer graphene/PEDOT:PSS-based OLEDs. Inset shows current efficiency versus current density of OLED devices. Reproduced with permission.[46] Copyright 2013, Elsevier. b) Luminance versus applied voltage for monolayer graphene and monolayer graphene/PEDOT:PSS-based OLEDs. Inset shows optical image of light emitting hybrid OLED. Reproduced with permission.[46] Copyright 2013, Elsevier. c) Sheet resistance versus bending times for graphene and double-layered graphene/PEDOT:PSS films. Inset shows image of flexible graphene/PEDOT:PSS film on PET substrate. Reproduced with permission.[153] Copyright 2014, Elsevier. d) Current density versus applied voltage for double-layered graphene/PEDOT:PSS-based OLEDs. Reproduced with permission.[153] Copyright 2014, Elsevier. e) Current efficiency versus applied voltage for double-layered graphene/PEDOT:PSS-based OLEDs. Reproduced with permission.[153] Copyright 2014, Elsevier. f) Current efficiency versus bending times for double-layered graphene/PEDOT:PSS-based OLEDs. Reproduced with permission.[153] Copyright 2014, Elsevier.

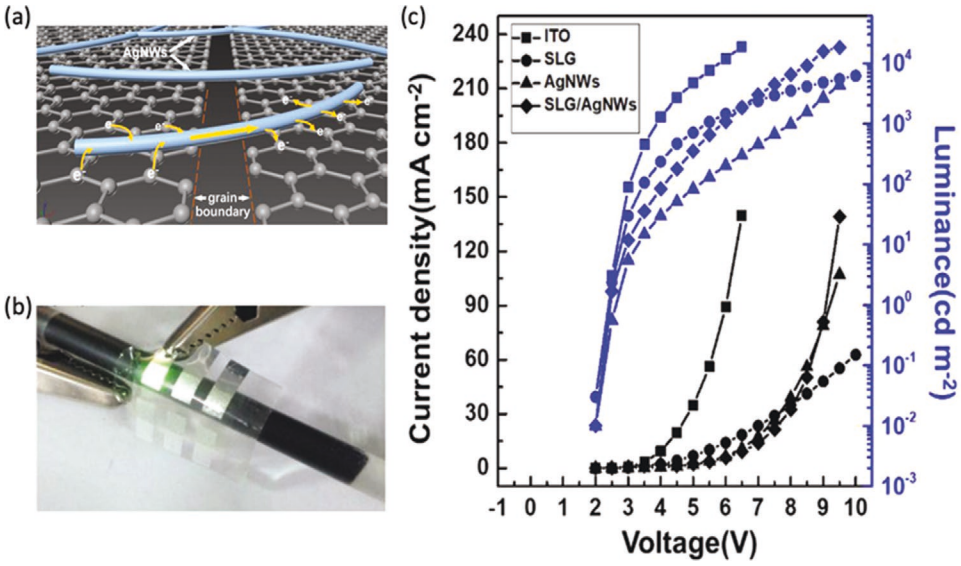


**Figure 18.** a) AgNWs providing conductive "bridges" between grain boundaries of graphene. b) Optical picture of flexible OLED with SLG/AgNWs hybrid electrode. c) Current density and luminance versus applied voltage for OLEDs with ITO, SLG, AgNWs, and SLG/AgNWs hybrid electrodes. Reproduced with permission.[144] Copyright 2019, Springer Nature.

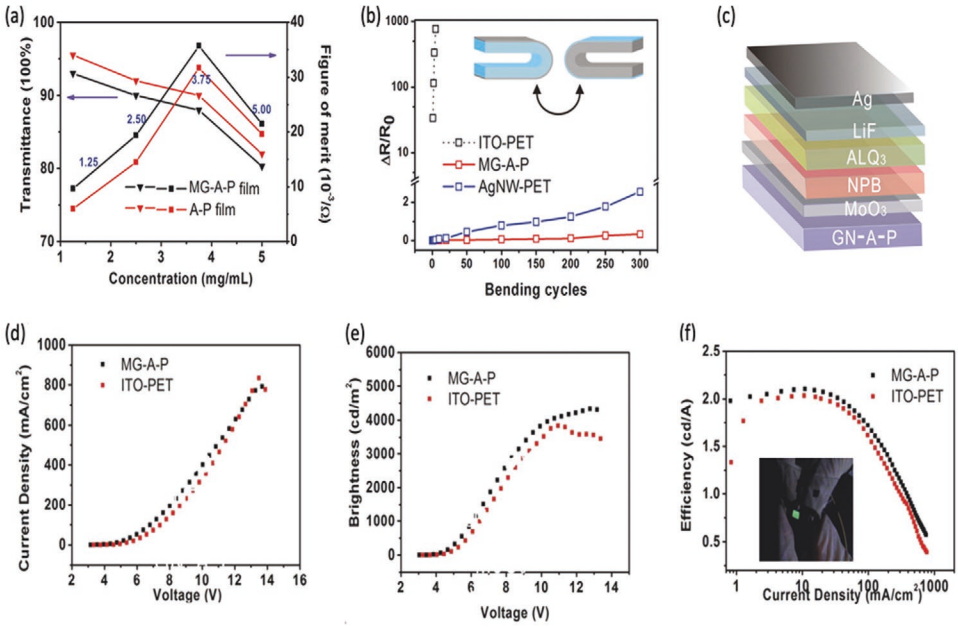


**Figure 19.** a) Transmittance at 550 nm and FOM versus AgNWs concentration for A–P and MG–A–P films. b) Changes in sheet resistance versus bending cycles for ITO-PET, MG–A–P, and AgNW-PET electrodes. Inset shows sample bending schematic. c) OLED device structure. d) Current density versus applied voltage of OLEDs based in MG–A–P and ITO-PET films. e) Brightness versus applied voltage of OLEDs based in MG–A–P and ITO-PET films. f) Current efficiency versus current density of OLEDs based in MG–A–P and ITO-PET films. Inset shows bright MG–A–P hybrid OLED device. Reproduced with permission.[47] Copyright 2016, American Chemical Society.

Numerous efforts focusing on the application of graphene-based TCEs in OLEDs have been made in recent years to improve their performance and efficiencies as discussed and summarized in **Table 3**. These studies display the superiority in the use of graphene-based TCEs in OLEDs when compared to conventional ITO. Presently, graphene films show improvements in their sheet resistance, WF, and transmittance when doped and combined with other materials to form a hybrid structure, however, they are still not perfect, and each enhancement technique have variations in performance when used in OLEDs. Reports suggests an improvement in OLED performance result from an enhanced electrical contact between graphene and other organic materials in OLEDs.[36,40,44,45,154,157] This can be attributed to their identical molecular structures which improves their bond strength and can enhance hole injection. The excellent mechanical flexibility of graphene-based OLEDs without loss in device performance when subjected to multiple bending cycles and graphene's cheaper synthesis method makes graphene an ideal TCE material that can be used for the development of flexible, stable, and enhanced OLED devices.

## 7. Conclusion and Outlook

The replacement of ITO with new materials such as conducting polymers, CNTs, metal nanostructures, and graphene has tremendously advanced the field of electronics due to their advantage of stability, flexibility, and improved performance in devices such as OLEDs. Specifically, graphene has received a lot of attention within the past decade due to its unique properties including high mechanical flexibility, high optical transparency, and low sheet resistance. In this review, we have summarized the progress of graphene-based TCEs and their application in OLEDs for performance improvements when compared to ITO. Several methods such as CVD and reduction of GO have been developed to synthesize graphene films for use as transparent conducting electrodes. Among many synthesis routes, the CVD technique has been the most prevalent technique since currently operated laboratory level technologies are now widely available to enable low-cost and high-throughput graphene film production. However, the challenge remains the lack of scalability, nonuniformity, and formation of defects in graphene films for use as TCEs in optoelectronic devices such as OLEDs. Current available technologies for graphene CVD growth still primarily utilizes copper substrates, resulting in graphene grain boundaries which lead to unwanted defects destroying the electronic properties of graphene films and degradation of devices. Several approaches have been taken to solve these issues by creating a conductive connection between the grain boundaries by using AgNWs, nonetheless, other issues still exist; graphene transfer is problematic due to the introduction of contaminations (defects), the use of etchants which are toxic and increases cost, time consuming, and poor adhesion of graphene to desired substrates. Graphene transfer can be eliminated if growth is directly on desired substrate or graphene can be synthesized on liquid substrates (gallium or tin) to take advantage of the weak van der Waals force between graphene layers and liquid metal substrates, enabling easy and smooth exfoliation.[166–169] To meet commercial industrial requirements for graphene use in optoelectronics, reasonable

**Table 3.** Characteristic performance of OLEDs with graphene-based TCE.

| Anode | Substrate | $V_{on}$ [a] [V] | Efficiencies | | | $L$ [e] [cd m$^{-2}$] | Ref. |
|---|---|---|---|---|---|---|---|
| | | | CE [b] [cd A$^{-1}$] | PE [c] [lm W$^{-1}$] | EQE [d] [%] | | |
| Graphene (four layer tandem) | Glass | – | 202.9 (max) | – | ≈44.4 (max) | ≈10 000 | [154] |
| | PET | – | 205.9 (max) | – | ≈45.2 (max) | | |
| Graphene (three layer) | Glass | 3.7 | 56.42 | – | – | ≈10 000 at 8.4 V | [155] |
| Graphene | Glass | 4.5 | – | ≈0.5 (max) | ≈0.4 (max) | 300 at 11.7 V | [40] |
| Graphene | PET | 2.5 | 111.4 (max) | 124.9 (max) | 29.7 | – | [156] |
| Graphene w/$O_2$ plasma | Glass | 3.9 | – | 24.1 | 15.6 | 1000 | [157] |
| Graphene (four layer)–$AuCl_3$ doped | PET | 2 | 27.4 (max) | 28.1 (max) | – | – | [36] |
| Graphene (four layer)–$HNO_3$ doped | PET | 2 | 30.2 (max) | 37.2 (max) | – | – | [36] |
| Graphene–$MoO_3$ doped | Glass | 2.5 | 55 (monolayer) | ≈34 | – | 1000 | [42] |
| | | | 67 (three layers) | ≈35 | | | |
| Graphene–$WO_3$ doped | Glass | >2.7 | – | 62 | – | 1000 | [43] |
| Graphene–boron doped | PET | – | 95.4 (max) | 99.7 (max) | 24.6 (max) | – | [41] |
| n-Doped graphene | Glass | 3.0 | 7 (max) | – | – | 19 020 at 27 V | [158] |
| Graphene | PET | 5 | 89.7 (max) | 102.6 | – | 10 000 | [159] |
| Graphene | Glass | 3.9 | 74.5 | 26.6 | 20.7 | 39 100 | [160] |
| Graphene/CNT with Au | Glass | 5 | 2.1 | – | – | 650 | [48] |
| Graphene–PMMA/SPPO1 | PET | 9.5 | 11.44 (max) | 2.24 (max) | – | – | [161] |
| Graphene/PEDOT:PSS | Glass | – | 0.89 (max) | – | – | 735.4 at 15 V | [46] |
| Graphene/PEDOT:PSS | PET | 5 | 0.91 (max) | – | – | – | [153] |
| Graphene/AgNWs | PET | 2.5 | – | – | – | 15 000 at 9 V | [144] |
| Graphene/AgNWs/CP | PET | 3.38 | 2.11 (max) | – | – | 4297 at 13 V | [47] |
| Graphene–fluoropolymer | Glass | 4.2 | 7.91 | – | – | – | [162] |
| Graphene–oligomer | Glass | 4.3 | 70 | – | – | 4250 at 9.5 V | [163] |
| Graphene//$TiO_x$/PEDOT:PSS | Glass | – | 10.11 | 5.41 | – | 1000 | [164] |
| $TiO_2$/graphene/CP | Glass | – | 168.4 | 160.3 | 40.8 | ≈500 at 5 V | [165] |

[a] $V_{on}$, turn-on voltage; [b] CE, current efficiency; [c] PE, power efficiency; [d] EQE, external quantum efficiency; [e] $L$, luminance.

advantages in terms of low-cost fabrication, large scale production, improved device performance, device stability, and reproducibility need to be met.

However, with these challenges come opportunities to developing new approaches to synthesizing graphene with improved optoelectronic properties, efficient and damage-free direct graphene transfer, production of high quality large-area graphene films, and improving uniformity. These are the areas in which future research should be targeted. Besides, strong adhesion to substrate, smooth surface morphology, excellent stability, enhanced mechanical flexibility, excellent performance, and long-lasting lifetime are required for highly flexible next-generation OLED devices utilizing graphene-based TCEs. Although, a few of the aforementioned challenges have been partially solved as discussed in this review, many obstacles still need to be conquered in the years to come for industrial-scale commercialization of flexible, foldable, and even stretchable OLEDs. We strongly believe that the field of graphene-based TCEs and their application in OLEDs is rapidly emerging, holding huge potential, and remains an active area of research where significant progress can be reached.

## Acknowledgements

A.E.A. acknowledges funding from the Dorothy Coker Research Fellowship, College of Science and Engineering, Texas State University and the Doctoral Research Support Fellowship, Graduate College, Texas State University. A.Z. acknowledges financial support from the National Science Foundation, EPMD program, Grant No. 1906492, and the U.S. Department of the Navy, HBCU/MI program, ONR award, Grant No. N000141912576. The authors acknowledge the editor's invitation to contribute to the special issue of Advanced Optical Materials under the title "Organic Electronics and Beyond."

## Conflict of Interest

The authors declare no conflict of interest.

## Keywords

electroluminescence, graphene, organic light emitting diodes, organic optoelectronic devices, transparent conducting electrodes

Received: December 7, 2020
Revised: February 6, 2021
Published online:

[1] C. W. Tang, S. A. VanSlyke, *Appl. Phys. Lett.* **1987**, *51*, 913.
[2] C. G. Granqvist, A. Hultåker, *Thin Solid Films* **2002**, *411*, 1.
[3] M. Morales-Masis, S. De Wolf, R. Woods-Robinson, J. W. Ager, C. Ballif, *Adv. Electron. Mater.* **2017**, *3*, 1600529.
[4] K. Saxena, V. K. Jain, D. S. Mehta, *Opt. Mater.* **2009**, *32*, 221.
[5] A. Kasry, M. E. l Ashry, R. A. Nistor, A. A. Bol, G. S. Tulevski, G. J. Martyna, D. M. Newns, *Thin Solid Films* **2012**, *520*, 4827.
[6] J. E. McCarthy, C. A. Hanley, L. J. Brennan, V. G. Lambertini, Y. K. Gun'ko, *J. Mater. Chem. C* **2014**, *2*, 764.
[7] S. De, T. M. Higgins, P. E. Lyons, E. M. Doherty, P. N. Nirmalraj, W. J. Blau, J. J. Boland, J. N. Coleman, *ACS Nano* **2009**, *3*, 1767.
[8] L. Hu, H. S. Kim, J.-Y. Lee, P. Peumans, Y. Cui, *ACS Nano* **2010**, *4*, 2955.
[9] D. P. Langley, G. Giusti, M. Lagrange, R. Collins, C. Jiménez, Y. Bréchet, D. Bellet, *Sol. Energy Mater. Sol. Cells* **2014**, *125*, 318.
[10] A. Du Pasquier, H. E. Unalan, A. Kanwal, S. Miller, M. Chhowalla, *Appl. Phys. Lett.* **2005**, *87*, 203511.
[11] E. J. López-Naranjo, L. J. González-Ortiz, L. M. Apátiga, E. M. Rivera-Muñoz, A. Manzano-Ramírez, *J. Nanomater.* **2016**, *2016*, 1.
[12] A. I. Hofmann, E. Cloutet, G. Hadziioannou, *Adv. Electron. Mater.* **2018**, *4*, 1700412.
[13] D. S. Hecht, L. Hu, G. Irvin, *Adv. Mater.* **2011**, *23*, 1482.
[14] M. Luo, Y. Liu, W. Huang, W. Qiao, Y. Zhou, Y. Ye, L.-S. Chen, *Micromachines* **2017**, *8*, 12.
[15] M. W. Rowell, M. A. Topinka, M. D. McGehee, *Appl. Phys. Lett.* **2006**, *88*, 233506.
[16] Z. Wu, Z. Chen, X. Du, J. M. Logan, J. Sippel, M. Nikolou, K. Kamaras, J. R. Reynolds, D. B. Tanner, A. F. Hebard, A. G. Rinzler, *Science* **2004**, *305*, 1273.
[17] J. Y. Lee, S. T. Connor, Y. Cui, P. Peumans, *Nano Lett.* **2008**, *8*, 689.
[18] H. Wu, L. Hu, M. W. Rowell, D. Kong, J. J. Cha, J. R. McDonough, J. Zhu, Y. Yang, M. D. McGehee, Y. Cui, *Nano Lett.* **2010**, *10*, 4242.
[19] L. Hu, H. Wu, Y. Cui, *MRS Bull.* **2011**, *36*, 760.
[20] H. Wu, D. Kong, Z. Ruan, P.-C. Hsu, S. Wang, Z. Yu, T. J. Carney, L. Hu, S. Fan, Y. Cui, *Nat. Nanotechnol.* **2013**, *8*, 421.
[21] S. Bae, H. Kim, Y. Lee, X. Xu, J.-S. Park, Y. Zheng, J. Balakrishnan, T. Lei, H. R. Kim, Y. Song, Y.-J. Kim, K. S. Kim, B. Özyilmaz, J.-H. Ahn, B. H. Hong, S. Iijima, *Nat. Nanotechnol.* **2010**, *5*, 574.
[22] K. Ellmer, *Nat. Photonics* **2012**, *6*, 809.
[23] S. Ye, A. R. Rathmell, Z. Chen, I. E. Stewart, B. J. Wiley, *Adv. Mater.* **2014**, *26*, 6670.
[24] Y. Xia, K. Sun, J. Ouyang, *Adv. Mater.* **2012**, *24*, 2436.
[25] D. Lee, H. Lee, Y. Ahn, Y. Jeong, D.-Y. Lee, Y. Lee, *Nanoscale* **2013**, *5*, 7750.
[26] L. Yu, C. Shearer, J. Shapter, *Chem. Rev.* **2016**, *116*, 13413.
[27] U. Lang, N. Naujoks, J. Dual, *Synth. Met.* **2009**, *159*, 473.
[28] Y. H. Kim, C. Sachse, M. L. Machala, C. May, L. Müller-Meskamp, K. Leo, *Adv. Funct. Mater.* **2011**, *21*, 1076.
[29] M. Vosgueritchian, D. J. Lipomi, Z. Bao, *Adv. Funct. Mater.* **2012**, *22*, 421.
[30] M. Gedda, D. Das, P. K. Iyer, G. U. Kulkarni, *Mater. Res. Express* **2020**, *7*, 54005.
[31] H. B. Lee, W. Y. Jin, M. M. Ovhal, N. Kumar, J. W. Kang, *J. Mater. Chem. C* **2019**, *7*, 1087.
[32] A. R. Madaria, A. Kumar, C. Zhou, *Nanotechnology* **2011**, *22*, 245201.
[33] J. L. Elechiguerra, L. Larios-Lopez, C. Liu, D. Garcia-Gutierrez, A. Camacho-Bragado, M. J. Yacaman, *Chem. Mater.* **2005**, *17*, 6042.
[34] Z. Chen, B. Cotterell, W. Wang, *Eng. Fract. Mech.* **2002**, *69*, 597.
[35] H. Z. Geng, K. K. Ki, P. S. Kang, S. L. Young, Y. Chang, H. L. Young, *J. Am. Chem. Soc.* **2007**, *129*, 7758.
[36] T.-H. Han, Y. Lee, M.-R. Choi, S.-H. Woo, S.-H. Bae, B. H. Hong, J.-H. Ahn, T.-W. Lee, *Nat. Photonics* **2012**, *6*, 105.
[37] S. R. Forrest, *Nature* **2004**, *428*, 911.
[38] L. Gomez De Arco, Y. Zhang, C. W. Schlenker, K. Ryu, M. E. Thompson, C. Zhou, *ACS Nano* **2010**, *4*, 2865.
[39] J. Wu, H. A. Becerril, Z. Bao, Z. Liu, Y. Chen, P. Peumans, *Appl. Phys. Lett.* **2008**, *92*, 263302.
[40] J. Wu, M. Agrawal, H. A. Becerril, Z. Bao, Z. Liu, Y. Chen, P. Peumans, *ACS Nano* **2010**, *4*, 43.
[41] T.-L. Wu, C.-H. Yeh, W.-T. Hsiao, P.-Y. Huang, M.-J. Huang, Y.-H. Chiang, C.-H. Cheng, R.-S. Liu, P.-W. Chiu, *ACS Appl. Mater. Interfaces* **2017**, *9*, 14998.
[42] J. Meyer, P. R. Kidambi, B. C. Bayer, C. Weijtens, A. Kuhn, A. Centeno, A. Pesquera, A. Zurutuza, J. Robertson, S. Hofmann, *Sci. Rep.* **2014**, *4*, 5380.
[43] P. R. Kidambi, C. Weijtens, J. Robertson, S. Hofmann, J. Meyer, *Appl. Phys. Lett.* **2015**, *106*, 063304.
[44] J. Hwang, H. K. Choi, J. Moon, J.-W. Shin, C. W. Joo, J.-H. Han, D.-H. Cho, J. W. Huh, S.-Y. Choi, J.-I. Lee, H. Y. Chu, *Mater. Res. Bull.* **2012**, *47*, 2796.
[45] T. Sun, Z. L. Wang, Z. J. Shi, G. Z. Ran, W. J. Xu, Z. Y. Wang, Y. Z. Li, L. Dai, G. G. Qin, *Appl. Phys. Lett.* **2010**, *96*, 133301.
[46] S. Shin, J. Kim, Y. H. Kim, S. Il Kim, *Curr. Appl. Phys.* **2013**, *13*, S144.
[47] H. Dong, Z. Wu, Y. Jiang, W. Liu, X. Li, B. Jiao, W. Abbas, X. Hou, *ACS Appl. Mater. Interfaces* **2016**, *8*, 31212.
[48] P. Kumar, K. L. Woon, W. S. Wong, M. S. Mohamed Saheed, Z. A. Burhanudin, *Synth. Met.* **2019**, *257*, 116186.
[49] T. M. Barnes, M. O. Reese, J. D. Bergeson, B. A. Larsen, J. L. Blackburn, M. C. Beard, J. Bult, J. van de Lagemaat, *Adv. Energy Mater.* **2012**, *2*, 353.
[50] S. De, P. J. King, P. E. Lyons, U. Khan, J. N. Coleman, *ACS Nano* **2010**, *4*, 7064.
[51] S. De, P. J. King, M. Lotya, A. O'Neill, E. M. Doherty, Y. Hernandez, G. S. Duesberg, J. N. Coleman, *Small* **2010**, *6*, 458.
[52] D. B. Fraser, H. D. Cook, *J. Electrochem. Soc.* **1972**, *119*, 1368.
[53] G. Haacke, *J. Appl. Phys.* **1976**, *47*, 4086.
[54] V. K. Jain, A. P. Kulshreshtha, *Sol. Energy Mater.* **1981**, *4*, 151.
[55] R. G. Gordon, *MRS Bull.* **2000**, *25*, 52.
[56] B. S. Shim, J. Zhu, E. Jan, K. Critchley, N. A. Kotov, *ACS Nano* **2010**, *4*, 3725.
[57] M. W. Rowell, M. D. McGehee, *Energy Environ. Sci.* **2011**, *4*, 131.
[58] A. Kaskela, A. G. Nasibulin, M. Y. Timmermans, B. Aitchison, A. Papadimitratos, Y. Tian, Z. Zhu, H. Jiang, D. P. Brown, A. Zakhidov, E. I. Kauppinen, *Nano Lett.* **2010**, *10*, 4349.
[59] H. Lee, M. Kim, I. Kim, H. Lee, *Adv. Mater.* **2016**, *28*, 4541.
[60] B. Geffroy, P. le Roy, C. Prat, *Polym. Int.* **2006**, *55*, 572.
[61] A. K. Geim, *Am. Assoc. Adv. Sci.* **2009**, *324*, 1530.
[62] S. V. Morozov, K. S. Novoselov, M. I. Katsnelson, F. Schedin, D. C. Elias, J. A. Jaszczak, A. K. Geim, *Phys. Rev. Lett.* **2008**, *100*, 016602.
[63] A. A. Balandin, S. Ghosh, W. Bao, I. Calizo, D. Teweldebrhan, F. Miao, C. N. Lau, *Nano Lett.* **2008**, *8*, 902.
[64] C. Lee, X. Wei, J. W. Kysar, J. Hone, *Science* **2008**, *321*, 385.
[65] G. Eda, Y.-Y. Lin, S. Miller, C.-W. Chen, W.-F. Su, M. Chhowalla, *Appl. Phys. Lett.* **2008**, *92*, 233305.
[66] G. Eda, G. Fanchini, M. Chhowalla, *Nat. Nanotechnol.* **2008**, *3*, 270.
[67] I. Jung, D. A. Dikin, R. D. Piner, R. S. Ruoff, *Nano Lett.* **2008**, *8*, 4283.
[68] W. S. Hummers, R. E. Offeman, *J. Am. Chem. Soc.* **1958**, *80*, 1339.
[69] K. S. Kim, Y. Zhao, H. Jang, S. Y. Lee, J. M. Kim, K. S. Kim, J.-H. Ahn, P. Kim, J.-Y. Choi, B. H. Hong, *Nature* **2009**, *457*, 706.
[70] Q. Yu, J. Lian, S. Siriponglert, H. Li, Y. P. Chen, S.-S. Pei, *Appl. Phys. Lett.* **2008**, *93*, 113103.
[71] X. Li, W. Cai, J. An, S. Kim, J. Nah, D. Yang, R. Piner, A. Velamakanni, I. Jung, E. Tutuc, S. K. Banerjee, L. Colombo, R. S. Ruoff, *Science* **2009**, *324*, 1312.

[72] Y. Zhu, S. Murali, W. Cai, X. Li, J. W. Suk, J. R. Potts, R. S. Ruoff, *Adv. Mater.* **2010**, *22*, 3906.
[73] R. K. Singh, R. Kumar, D. P. Singh, *RSC Adv.* **2016**, *6*, 64993.
[74] A. Adetayo, D. Runsewe, *Open J. Compos. Mater.* **2019**, *09*, 207.
[75] C. Zhu, S. Guo, Y. Fang, S. Dong, *ACS Nano* **2010**, *4*, 2429.
[76] P. W. Sutter, J.-I. Flege, E. A. Sutter, *Nat. Mater.* **2008**, *7*, 406.
[77] J. Coraux, A. T. N'Diaye, C. Busse, T. Michely, *Nano Lett.* **2008**, *8*, 565.
[78] A. N. Obraztsov, E. A. Obraztsova, A. V. Tyurnina, A. A. Zolotukhin, *Carbon* **2007**, *45*, 2017.
[79] Y. Chen, X. L. Gong, J. G. Gai, *Adv. Sci.* **2016**, *3*, 1500343.
[80] X. Chen, L. Zhang, S. Chen, *Synth. Met.* **2015**, *210*, 95.
[81] A. Reina, X. Jia, J. Ho, D. Nezich, H. Son, V. Bulovic, M. S. Dresselhaus, J. Kong, *Nano Lett.* **2009**, *9*, 30.
[82] S. Chen, W. Cai, R. D. Piner, J. W. Suk, Y. Wu, Y. Ren, J. Kang, R. S. Ruoff, *Nano Lett.* **2011**, *11*, 3519.
[83] X. Liu, L. Fu, N. Liu, T. Gao, Y. Zhang, L. Liao, Z. Liu, *J. Phys. Chem. C* **2011**, *115*, 11976.
[84] T. Wu, X. Zhang, Q. Yuan, J. Xue, G. Lu, Z. Liu, H. Wang, H. Wang, F. Ding, Q. Yu, X. Xie, M. Jiang, *Nat. Mater.* **2016**, *15*, 43.
[85] Y. Wu, H. Chou, H. Ji, Q. Wu, S. Chen, W. Jiang, Y. Hao, J. Kang, Y. Ren, R. D. Piner, R. S. Ruoff, *ACS Nano* **2012**, *6*, 7731.
[86] W.-H. Lin, T.-H. Chen, J.-K. Chang, J.-I. Taur, Y.-Y. Lo, W.-L. Lee, C.-S. Chang, W.-B. Su, C.-I. Wu, *ACS Nano* **2014**, *8*, 1784,.
[87] M.-S. Lee, K. Lee, S.-Y. Kim, H. Lee, J. Park, K.-H. Choi, H.-K. Kim, D.-G. Kim, D.-Y. Lee, S. Nam, J.-U. Park, *Nano Lett.* **2013**, *13*, 2814.
[88] D.-Y. Wang, I.-S. Huang, P.-H. Ho, S.-S. Li, Y.-C. Yeh, D.-W. Wang, W.-L. Chen, Y.-Y. Lee, Y.-M. Chang, C.-C. Chen, C.-T. Liang, C.-W. Chen, *Adv. Mater.* **2013**, *25*, 4521.
[89] J. W. Suk, A. Kitt, C. W. Magnuson, Y. Hao, S. Ahmed, J. An, A. K. Swan, B. B. Goldberg, R. S. Ruoff, *ACS Nano* **2011**, *5*, 6916.
[90] C. Yan, J. H. Cho, J.-H. Ahn, *Nanoscale* **2012**, *4*, 4870.
[91] A. V. Zaretski, D. J. Lipomi, *Nanoscale* **2015**, *7*, 9963.
[92] A. V. Zaretski, H. Moetazedi, C. Kong, E. J. Sawyer, S. Savagatrup, E. Valle, T. F. O'Connor, A. D. Printz, D. J. Lipomi, *Nanotechnology* **2015**, *26*, 045301.
[93] Y. Lee, S. Bae, H. Jang, S. Jang, S.-E. Zhu, S. H. Sim, Y. Song, B. H. Hong, J.-H. Ahn, *Nano Lett.* **2010**, *10*, 490.
[94] A. Reina, H. Son, L. Jiao, B. Fan, M. S. Dresselhaus, Z. Liu, J. Kong, *J. Phys. Chem. C* **2008**, *112*, 17741.
[95] M. P. Levendorf, C. S. Ruiz-Vargas, S. Garg, J. Park, *Nano Lett.* **2009**, *9*, 4479.
[96] J. Sun, Z. Chen, L. Yuan, Y. Chen, J. Ning, S. Liu, D. Ma, X. Song, M. K. Priydarshi, A. Bachmatiuk, M. H. Rümmeli, T. Ma, L. Zhi, L. Huang, Y. Zhang, Z. Liu, *ACS Nano* **2016**, *10*, 11136.
[97] N. Liu, Z. Pan, L. Fu, C. Zhang, B. Dai, Z. Liu, *Nano Res.* **2011**, *4*, 996.
[98] C. Cai, F. Jia, A. Li, F. Huang, Z. Xu, L. Qiu, Y. Chen, G. Fei, M. Wang, *Carbon* **2016**, *98*, 457.
[99] B. N. Chandrashekar, B. Deng, A. S. Smitha, Y. Chen, C. Tan, H. Zhang, H. Peng, Z. Liu, *Adv. Mater.* **2015**, *27*, 5210.
[100] J. Sun, Y. Chen, X. Cai, B. Ma, Z. Chen, M. K. Priydarshi, K. Chen, T. Gao, X. Song, Q. Ji, X. Guo, D. Zou, Y. Zhang, Z. Liu, *Nano Res.* **2015**, *8*, 3496.
[101] J. Sun, Y. Chen, M. K. Priydarshi, Z. Chen, A. Bachmatiuk, Z. Zou, Z. Chen, X. Song, Y. Gao, M. H. Rümmeli, Y. Zhang, Z. Liu, *Nano Lett.* **2015**, *15*, 5846.
[102] W. Xiong, Y. S. Zhou, L. J. Jiang, A. Sarkar, M. Mahjouri-Samani, Z. Q. Xie, Y. Gao, N. J. Ianno, L. Jiang, Y. F. Lu, *Adv. Mater.* **2013**, *25*, 630.
[103] X. Wang, L. Zhi, K. Müllen, *Nano Lett.* **2008**, *8*, 323.
[104] Q. Zheng, Z. Li, J. Yang, J.-K. Kim, *Prog. Mater. Sci.* **2014**, *64*, 200.
[105] K. P. Loh, Q. Bao, G. Eda, M. Chhowalla, *Nat. Chem.* **2010**, *2*, 1015.
[106] S. Das, P. Sudhagar, Y. S. Kang, W. Choi, in *Carbon Nanomaterials for Advanced Energy Systems* (Eds: W. Lu, J.-B. Baek, L. Dai), John Wiley & Sons, Inc, Hoboken, NJ **2015**, pp. 85–131.
[107] L. Staudenmaier, *Eur. J. Inorg. Chem.* **1898**, *31*, 1481.
[108] S. Gilje, S. Han, M. Wang, K. L. Wang, R. B. Kaner, *Nano Lett.* **2007**, *7*, 3394.
[109] H. A. Becerril, J. Mao, Z. Liu, R. M. Stoltenberg, Z. Bao, Y. Chen, *ACS Nano* **2008**, *2*, 463.
[110] L. J. Cote, F. Kim, J. Huang, *J. Am. Chem. Soc.* **2009**, *131*, 1043.
[111] D. Li, M. B. Müller, S. Gilje, R. B. Kaner, G. G. Wallace, *Nat. Nanotechnol.* **2008**, *3*, 101.
[112] V. H. Pham, T. V. Cuong, S. H. Hur, E. W. Shin, J. S. Kim, J. S. Chung, E. J. Kim, *Carbon* **2010**, *48*, 1945.
[113] I. K. Moon, J. Lee, R. S. Ruoff, H. Lee, *Nat. Commun.* **2010**, *1*, 73.
[114] C. K. Chua, M. Pumera, *Chem. Soc. Rev.* **2014**, *43*, 291.
[115] C. Gómez-Navarro, J. C. Meyer, R. S. Sundaram, A. Chuvilin, S. Kurasch, M. Burghard, K. Kern, U. Kaiser, *Nano Lett.* **2010**, *10*, 1144.
[116] X. Gao, J. Jang, S. Nagase, *J. Phys. Chem. C* **2010**, *114*, 832.
[117] A. Viinikanoja, Z. Wang, J. Kauppila, C. Kvarnström, *Phys. Chem. Chem. Phys.* **2012**, *14*, 14003.
[118] K. Krishnamoorthy, M. Veerapandian, G.-S. Kim, S. J. Kim, *Curr. Nanosci.* **2012**, *8*, 934.
[119] Z. Dai, K. Wang, L. Li, T. Zhang, *Int. J. Electrochem. Sci.* **2013**, *8*, 9384
[120] A. L. Stroyuk, N. S. Andryushina, N. D. Shcherban', V. G. Il'in, V. S. Efanov, I. B. Yanchuk, S. Ya Kuchmii, V. D. Pokhodenko, *Theor. Exp. Chem.* **2012**, *48*, 2.
[121] A. Kasry, M. A. Kuroda, G. J. Martyna, G. S. Tulevski, A. A. Bol, *ACS Nano* **2010**, *4*, 3839.
[122] H. Liu, Y. Liu, D. Zhu, *J. Mater. Chem.* **2011**, *21*, 3335.
[123] Q. Zheng, W. H. Ip, X. Lin, N. Yousefi, K. K. Yeung, Z. Li, J.-K. Kim, *ACS Nano* **2011**, *5*, 6039.
[124] W. Cai, Y. Zhu, X. Li, R. D. Piner, R. S. Ruoff, *Appl. Phys. Lett.* **2009**, *95*, p. 123115.
[125] K. K. Walsh, C. Murphy, G. Jones, M. Barnes, A. D. Sanctis, D.-W. Shin, S. Russo, M. Craciun, *Photonics Sol. Energy Syst. VII* **2018**, *10688*, 52.
[126] K. K. Kim, A. Reina, Y. Shi, H. Park, L.-J. Li, Y. H. Lee, J. Kong, *Nanotechnology* **2010**, *21*, 285205.
[127] J. M. Kim, S. Kim, D. H. Shin, S. W. Seo, H. S. Lee, J. H. Kim, C. W. Jang, S. S. Kang, S.-H. Choi, G. Y. Kwak, K. J. Kim, H. Lee, H. Lee, *Nano Energy* **2018**, *43*, 124.
[128] S. J. Lee, Y. R. Lim, S. Ji, S. K. Kim, Y. Yoon, W. Song, S. Myung, J. Lim, K.-S. An, J.-S. Park, S. S. Lee, *Carbon* **2018**, *126*, 241.
[129] J. Wan, F. Gu, W. Bao, J. Dai, F. Shen, W. Luo, X. Han, D. Urban, L. Hu, *Nano Lett.* **2015**, *15*, 3763.
[130] L. La Notte, G. V. Bianco, A. L. Palma, A. Di Carlo, G. Bruno, A. Reale, *Carbon* **2018**, *129*, pp. 878.
[131] Y. Wang, X. Chen, Y. Zhong, F. Zhu, K. P. Loh, *Appl. Phys. Lett.* **2009**, *95*, 063302.
[132] A. E. Mansour, S. Dey, A. Amassian, M. H. Tanielian, *ACS Appl. Mater. Interfaces* **2015**, *7*, 17692.
[133] E. S. M. Duraia, A. Fahami, G. W. Beall, *J. Electron. Mater.* **2018**, *47*, 1176.
[134] Y. Xu, H. Yu, C. Wang, J. Cao, Y. Chen, Z. Ma, Y. You, J. Wan, X. Fang, X. Chen, *Nanoscale Res. Lett.* **2017**, *12*, 254.
[135] I. Khrapach, F. Withers, T. H. Bointon, D. K. Polyushkin, W. L. Barnes, S. Russo, M. F. Craciun, *Adv. Mater.* **2012**, *24*, 2844.
[136] C.-L. Hsu, C.-T. Lin, J.-H. Huang, C.-W. Chu, K.-H. Wei, L.-J. Li, *ACS Nano* **2012**, *6*, 5031.
[137] I. Jo, Y. Kim, J. Moon, S. Park, J. S. Moon, W. B. Park, J. S. Lee, B. H. Hong, *Phys. Chem. Chem. Phys.* **2015**, *17*, 29492.

[138] P. Blake, P. D. Brimicombe, R. R. Nair, T. J. Booth, D. Jiang, F. Schedin, L. A. Ponomarenko, S. V. Morozov, H. F. Gleeson, E. W. Hill, A. K. Geim, K. S. Novoselov, *Nano Lett.* **2008**, *8*, 1704.
[139] S. H. Kim, W. Song, M. W. Jung, M.-A. Kang, K. Kim, S.-J. Chang, S. S. Lee, J. Lim, J. Hwang, S. Myung, K.-S. An, *Adv. Mater.* **2014**, *26*, 4247.
[140] P. J. King, U. Khan, M. Lotya, S. De, J. N. Coleman, *ACS Nano* **2010**, *4*, 4238.
[141] R. Chen, S. R. Das, C. Jeong, M. R. Khan, D. B. Janes, M. A. Alam, *Adv. Funct. Mater.* **2013**, *23*, 5150.
[142] Y.-K. Kim, D.-H. Min, *Langmuir* **2009**, *25*, 11302.
[143] H.-G. Im, S.-H. Jung, J. Jin, D. Lee, J. Lee, D. Lee, J.-Y. Lee, I.-D. Kim, B.-S. Bae, *ACS Nano* **2014**, *8*, 10973.
[144] H. Li, Y. Liu, A. Su, J. Wang, Y. Duan, *Sci. Rep.* **2019**, *9*, 17998.
[145] Y. Zhu, Z. Sun, Z. Yan, Z. Jin, J. M. Tour, *ACS Nano* **2011**, *5*, 6472.
[146] B. Deng, P.-C. Hsu, G. Chen, B. N. Chandrashekar, L. Liao, Z. Ayitimuda, J. Wu, Y. Guo, L. Lin, Y. Zhou, M. Aisijiang, Q. Xie, Y. Cui, Z. Liu, H. Peng, *Nano Lett.* **2015**, *15*, 4206.
[147] Y. Ahn, Y. Jeong, Y. Lee, *ACS Appl. Mater. Interfaces* **2012**, *4*, 6410.
[148] K. Jo, T. Lee, H. J. Choi, J. H. Park, D. J. Lee, D. W. Lee, B.-S. Kim, *Langmuir* **2011**, *27*, 2014.
[149] B. H. Lee, J.-H. Lee, Y. H. Kahng, N. Kim, Y. J. Kim, J. Lee, T. Lee, K. Lee, *Adv. Funct. Mater.* **2014**, *24*, 1847.
[150] Z. Liu, K. Parvez, R. Li, R. Dong, X. Feng, K. Müllen, *Adv. Mater.* **2015**, *27*, 669.
[151] V. C. Tung, L.-M. Chen, M. J. Allen, J. K. Wassei, K. Nelson, R. B. Kaner, Y. Yang, *Nano Lett.* **2009**, *9*, 1949.
[152] Q. Zheng, B. Zhang, X. Lin, X. Shen, N. Yousefi, Z.-D. Huang, Z. Li, J.-K. Kim, *J. Mater. Chem.* **2012**, *22*, 25072.
[153] X. Wu, F. Li, W. Wu, T. Guo, *Appl. Surf. Sci.* **2014**, *295*, 214.
[154] T.-H. Han, M.-H. Park, S.-J. Kwon, S.-H. Bae, H.-K. Seo, H. Cho, J.-H. Ahn, T.-W. Lee, *NPG Asia Mater* **2016**, *8*, 303.
[155] I.-J. Park, T. I. Kim, T. Yoon, S. Kang, H. Cho, N. S. Cho, J.-I. Lee, T.-S. Kim, S.-Y. Choi, *Adv. Funct. Mater.* **2018**, *28*, 1704435.
[156] L. P. Ma, Z. Wu, L. Yin, D. Zhang, S. Dong, Q. Zhang, M.-L. Chen, W. Ma, Z. Zhang, J. Du, D.-M. Sun, K. Liu, X. Duan, D. Ma, H.-M. Cheng, W. Ren, *Proc. Natl. Acad. Sci. USA* **2020**, *117*, 25991.
[157] J. Hwang, H. K. Choi, J. Moon, T. Y. Kim, J.-W. Shin, C. W. Joo, J.-H. Han, D.-H. Cho, J. W. Huh, S.-Y. Choi, J.-I. Lee, H. Y. Chu, *Appl. Phys. Lett.* **2012**, *100*, 133304.
[158] J. O. Hwang, J. S. Park, D. S. Choi, J. Y. Kim, S. H. Lee, K. E. Lee, Y.-H. Kim, M. H. Song, S. Yoo, S. O. Kim, *ACS Nano* **2012**, *6*, 159.
[159] Z. Zhang, J. Du, D. Zhang, H. Sun, L. Yin, L. Ma, J. Chen, D. Ma, H.-M. Cheng, W. Ren, *Nat. Commun.* **2017**, *8*, 14560.
[160] L. Liu, W. Shang, C. Han, Q. Zhang, Y. Yao, X. Ma, M. Wang, H. Yu, Y. Duan, J. Sun, S. Chen, W. Huang, *ACS Appl. Mater. Interfaces* **2018**, *10*, 7289.
[161] Y. Han, L. Zhang, X. Zhang, K. Ruan, L. Cui, Y. Wang, L. Liao, Z. Wang, J. Jie, *J. Mater. Chem. C* **2014**, *2*, 201.
[162] K. C. Kwon, S. Kim, C. Kim, J.-L. Lee, S. Y. Kim, *Org. Electron.* **2014**, *15*, 3154.
[163] N. Mustapha, Z. Fekkai, K. H. Ibnaouf, *J. Electron. Mater.* **2020**, *49*, 2203.
[164] X.-Z. Zhu, Y.-Y. Han, Y. Liu, K.-Q. Ruan, M.-F. Xu, Z.-K. Wang, J.-S. Jie, L.-S. Liao, *Org. Electron.* **2013**, *14*, 3348.
[165] J. Lee, T.-H. Han, M.-H. Park, D. Y. Jung, J. Seo, H.-K. Seo, H. Cho, E. Kim, J. Chung, S.-Y. Choi, T.-S. Kim, T.-W. Lee, S. Yoo, *Nat. Commun.* **2016**, *7*, 11791.
[166] G. Ding, Y. Zhu, S. Wang, Q. Gong, L. Sun, T. Wu, X. Xie, M. Juang, *Carbon* **2013**, *53*, 321.
[167] M. Zeng, L. Tan, J. Wang, L. Chen, M. H. Rümmeli, L. Fu, *Chem. Mater.* **2014**, *26*, 3637.
[168] M. Zeng, L. Fu, *Acc. Chem. Res.* **2018**, *51*, 2839.
[169] N. R. Glavin, C. Muratore, M. Snure, *Oxford Open Mater. Sci.* **2020**, *1*, 1.

**Adeniji E. Adetayo** received his B.Eng. degree in chemical engineering from Covenant University, Nigeria, in 2013 and his M.Sc.Eng. degree in chemical engineering from Lamar University, USA, in 2017. Currently, he is a Ph.D. candidate in materials science, engineering, and commercialization program under the supervision of Dr. Gary Beall at Texas State University, USA. His research is mainly focused on the development and synthesis of 2D graphene materials, and their application in optoelectronic devices and composites.

**Tanjina N. Ahmed** is currently pursuing her Ph.D. in materials science, engineering, and commercialization program at Texas State University, USA. She received her M.Sc. degree in physics from Western Illinois University, USA, in 2018. Tanjina holds an M.Phil. degree in physics from Bangladesh University of Engineering and Technology (BUET) and graduated from University of Dhaka with her B.Sc. degree in physics. She possesses a materials physics background in the area of thin film fabrication and device characterization. Currently, her research is focused on 3D-printed magnetic polymer composite materials and their properties for application in permanent magnet and electromagnetic devices.

**Alex Zakhidov** is an associate professor of physics and core faculty in materials science, engineering, and commercialization Ph.D. program at Texas State University. He earned his Ph.D. degree in solid-state physics from Moscow State University, Russia, in 2006. After a post-doctoral fellowship at Cornell University and Alexander Von Humboldt Fellowship in Technical University of Dresden, Germany, he joined Texas State in 2014. His current research interests are in theoretical and experimental study of organic and hybrid semiconductors, including fundamentals, processing mechanisms, and applications in optoelectronics.

**Gary W. Beall** obtained his Ph.D. degree in physical chemistry from Baylor University, USA, in 1975. Afterward, he joined Oak Ridge National Laboratory where he conducted research on the environmental fate of actinides. He then moved to industry for 21 years. The research conducted during this period involved application of surface-modified clay nanoparticles in a wide variety of commercial products. He is currently full professor in the Department of Chemistry and Biochemistry, Regents' Professor, and Formosa Endowed Chair at Texas State University. His recent research interests include low-cost synthesis of graphenes and other 2D materials.